Energy Strategy Reviews 44 (2022) 101014

Contents lists available at ScienceDirect

Energy Strategy Reviews

journal homepage: www.elsevier.com/locate/esr

Decarbonizing the electricity sector in Qatar using PV combined with ice thermal and battery storage

I. Al-Aali *, V. Modi

Mechanical Engineering Department, Columbia University, New York City, United States

ARTICLE INFO

Keywords:
Ice storage
Battery energy storage system
Solar photovoltaic
Deep decarbonization solutions
High renewables penetration
Sustainability
Cooling load decarbonization
Qatar energy

ABSTRACT

High daytime electricity demand from space cooling synergetic with predictable and reliable solar insolation creates a unique opportunity to exploit solar PV-enabled decarbonization solutions in Qatar. This paper examines the economic viability of combining utility-scale PV with ice thermal and battery storage to decarbonize the electricity sector in Qatar, which exclusively runs on gas generation. The problem is formulated in a two-stage stochastic linear programming that minimizes annual system costs at a given gas price. Under the current gas price of $3.3/MMBtu (gas-generated electricity at $37/MWh), PV and ice storage deployed in Qatar could reduce gas generation use and peak demand by 43% and 18%, respectively, and cut the annual system costs by 20%. At a gas price of $6.5/MMBtu (equivalent to carbon pricing at $60/ton of CO_2), gas generation can be reduced by 60% using PV and ice storage. Reducing gas generation further is challenging since both cooling and non-cooling demands peak in August, whereas PV generation peaks in June, producing less surplus generation at a time of need, and ice thermal storage cannot cost-effectively outcompete already existing gas generations for highly seasonal cooling needs. Battery storage becomes cost-effective above a gas price of $9.2/MMBtu (equivalent to carbon pricing at $110/ton of CO_2); it is primarily used to manage the diurnal behavior of non-cooling loads and could decarbonize the electricity sector by around 90%.

1. Introduction

Qatar is a small country along the Arabian Gulf with a population of 2.9 million and a total land area of 11,600 km^2. The climate can be described as dry-arid with mild winter months (average daily temperature of 20–25 $^\circ C$) and hot summer months (average daily temperature of 35–40 $^\circ C$). Qatar ranks highest for per capita carbon emissions [1]. Although largely propelled by carbon emissions from producing and exporting liquefied natural gas, it displaces dirtier and more emission-producing fuels elsewhere. Still, the electricity sector is responsible for one-fourth of total carbon emissions, of which buildings account for 60% of total electricity use [1,2]. The high electricity demands in buildings are dominated by near year-round energy-intensive space-cooling [3,4]. Qatar's electricity and water demands are met by gas-fired integrated water and power plants, combining electricity production and water desalination. The total electricity and desalinated water consumption in 2016 were 42 TWh and 560 million m^3, respectively, produced using 452 million MMBtu of natural gas and emitting 24 Mt of CO_2 [2].

Electricity is subsidized based on sector and consumption bracket [5]. For residential, commercial, and industrial customers with a monthly consumption bracket of less than 4 MWh, the rate is flat at $36/MWh. For bulk customers with a peak demand greater than 5 MW, the tariff is $58/MWh during the low-demand seasons and rises to $93/MWh during peak hours in the hotter months (May to October) from 12 to 6 p.m. [5]. The on-peak pricing is motivated by the growing peak demand, which grew at an average rate of 6%/yr. since 2010 to 7.33 GW in 2016. This led to expanding gas generation capacity only to supplement the yearly marginal increase in demand in the hotter summer months. Also, the high ambient temperatures in the summer significantly depress their power capacity and thermal efficiency relative to their design condition, further upsizing them. Fig. 1 shows Qatar's daily electricity demand and ambient temperatures for three consecutive days in the winter (January 5–7), spring (April 10–12), and summer (September 2–4), which were generated using 2016 datasets.

Abbreviations: AC, Air-Cooled; AC CWS, Air-Cooled Chilled Water System; BESS, Battery Energy Storage System; Capex, Capital Expenditure; COP, Coefficient of Performance; CWS, Chilled Water System; D, Demand; DD, Demand Directly; DXS, Direct Expansion System; I-TES, Ice Thermal Energy Storage; OpEx, Operation Expenditure; PV, Photovoltaics; TR, Ton of Refrigeration; WC, Water-Cooled; WC CWS, Water-Cooled Chilled Water System.

* Corresponding author.
E-mail addresses: iaa2111@columbia.edu (I. Al-Aali), vm2@columbia.edu (V. Modi).

https://doi.org/10.1016/j.esr.2022.101014
Received 7 July 2022; Received in revised form 7 November 2022; Accepted 23 November 2022
Available online 26 November 2022

Parameters

$HR_{p,t}$ Humidity ratio at time t and scenario p, [kg of water/kg of air]

$B_{p,t}$ Logistic curve non-cooling load at time t and scenario p, [MW]

$\mathscr{C}^{DX}_{p,t}$ Hourly aggregate thermal cooling demand from direct expansion systems at time t and scenario p, [MW_{th}]

$\mathscr{C}^{AC}_{p,t}$ Hourly aggregate thermal cooling demand from air-cooled chilled water systems at time t and scenario p, [MW_{th}]

$\mathscr{C}^{WC}_{p,t}$ Hourly aggregate thermal cooling demand from water-cooled chilled water systems at time t and scenario p, [MW_{th}]

C^{AC} Existing aggregate cooling capacity of air-cooled chilled water systems in refrigeration mode, [MW_{th}]

C^{WC} Existing aggregate cooling capacity of water-cooled chilled water systems in refrigeration mode, [MW_{th}]

$C^{AC,ice}$ Existing aggregate cooling capacity of air-cooled chilled water systems in ice-making mode, [MW_{th}]

$C^{WC,ice}$ Existing aggregate cooling capacity of water-cooled chilled water systems in ice-making mode, [MW_{th}]

$C^{DX,des}$ Design aggregate cooling capacity of existing direct expansion cooling systems, [MW_{th}]

$C^{AC,des}$ Design aggregate cooling capacity of existing air-cooled chilled water systems, [MW_{th}]

$C^{WC,des}$ Design aggregate cooling capacity of existing water-cooled chilled water systems, [MW_{th}]

$COP^{ac}_{p,t}$ Air-cooled systems coefficient of performance in refrigeration mode at time t and scenario p, dimensionless

$COP^{wc}_{p,t}$ Water-cooled systems coefficient of performance in refrigeration mode at time t and scenario p, dimensionless

$COP^{ac,ice}_{p,t}$ Air-cooled systems coefficient of performance in ice-making mode at time t and scenario p, dimensionless

$COP^{wc,ice}_{p,t}$ Water-cooled systems coefficient of performance in ice-making mode at time t and scenario p, dimensionless

$COP^{ac,des}_{p,t,i}$ Air-cooled systems design coefficient of performance at time t and scenario p, dimensionless

$COP^{wc,des}_{p,t}$ Water-cooled systems design coefficient of performance at time t and scenario p, dimensionless

c^{BESS} Capital cost of installed battery capacity, [$/MWh]

$c^{PV,C}_s$ Capital cost of installed PV capacity with solar tracking technology s, [$/$MW_{p,dc}$]

c^{ITES} Capital cost of installed ice storage capacity, [$/$MWh_{th}$]

$c^{IceChl,C}$ Capital cost of additionally installed ice chillers capacity, [$/$MW_{th}$]

$c^{PV,O}_s$ Operating cost of installed PV capacity with solar tracking technology s, [$/$MW_{p,dc}$/yr.]

$c^{IceChl,O}$ Operating cost of additionally installed ice chillers, [$/$MW_{th}$/yr.]

c^{GT} Cost of electricity produced by gas-fired generations , [$/MWh]

c^{PGT} Peak gas-fired generations demand price , [$/$MW_p$]

$\mathscr{D}_{p,t}$ Hourly aggregate total electric demand at time t and scenario p, [MW]

$\mathscr{D}^{\mathscr{N}}_{p,t}$ Hourly aggregate non-cooling electric demand at time t and scenario p, [MW]

$\mathscr{D}^{\mathscr{C}}_{p,t}$ Hourly aggregate total electric cooling load at time t and scenario p, [MW]

$\mathscr{D}^{DX}_{p,t}$ Hourly aggregate electric cooling load from direct expansion systems at time t and scenario p, [MW]

$\mathscr{D}^{AC}_{p,t}$ Hourly aggregate electric cooling load from air-cooled chilled water systems at time t and scenario p, [MW]

$\mathscr{D}^{WC}_{p,t}$ Hourly aggregate electric cooling load from water-cooled chilled water systems at time t and scenario p, [MW]

E^{DX} Maximum aggregate electric load from existing direct expansion cooling systems, [MW]

E^{AC} Maximum aggregate electric load from existing air-cooled chilled water systems, [MW]

E^{WC} Maximum aggregate electric load from existing water-cooled chilled water systems, [MW]

$f^{ITES,chs}$ Ice storage maximum charge power to energy ratio, [h^{-1}]

$f^{ITES,dis}$ Ice storage maximum discharge power to energy ratio, [h^{-1}]

$HI^0_{p,t}$ Logistic curve heat index midpoint at time t and scenario p, [$^\circ C$]

$HI_{p,t}$ Heat index at time t and scenario p, [$^\circ C$]

$I_{p,t,s}$ Hourly solar insolation with a solar tracking technology s at time t and scenario p, dimensionless by peak sun hour, [MW/MW_p]

ir Interest rate, dimensionless

$k_{p,t}$ Logistic curve slope at time t and scenario p, [$^\circ C^{-1}$]

$P_{p,t}$ Logistic curve peak demand at time t and scenario p, [MW]

$T^{db}_{p,t}$ Ambient dry-bulb temperature at time t and scenario p, [$^\circ C$]

$T^{wb}_{p,t}$ Ambient wet-bulb temperature at time t and scenario p, [$^\circ C$]

yr Service life of PV, ice chillers, and ice storage, [yrs.]

yrb Battery service life, [yrs.]

$\eta^{ITES,sdis}$ Ice storage self-discharge efficiency, dimensionless

$\eta^{BESS,chs}$ Battery charge efficiency, dimensionless

$\eta^{BESS,dis}$ Battery discharge efficiency, dimensionless

$\eta^{BESS,sdis}$ Battery self-discharge efficiency, dimensionless

η^{I} Inverter efficiency, dimensionless

ψ^{ice} Depressed chiller capacity factor in ice-making mode, dimensionless

φ^{ice} Depressed chiller performance factor in ice-making mode, dimensionless

Decision variables

$\mathscr{B}^{dis}_{p,t}$ Battery discharge rate at time t and scenario p, [MW]

$\mathscr{B}^{chs}_{p,t}$ Battery charge rate at time t and scenario p, [MW]

$\mathscr{B}^{s}_{p,t}$ Stored electric energy at time t and scenario p, [MWh]

C^{BESS} Installed electric battery capacity, [MWh]

C^{PV}_s Installed PV capacity with solar tracking technology s, [$MW_{p,dc}$]

C^{ITES}_i Installed ice storage thermal capacity for cooling system i, [MWh_{th}]

C^{IceChl}_i Additionally installed ice chiller capacity for cooling system i, [MW_{th}]

$GT_{p,t}$ Electricity generated from gas at time t and scenario p, [MW]

GT^{P} Peak gas generation demand, [MW]

$PV^{curt}_{p,t}$ Curtailed PV generation at time t and scenario p, [MW]

$S^{dis}_{p,t,i}$ Ice storage discharge rate for cooling system i at time t and scenario p, [MW_{th}]

$S^{ac,chs}_{p,t,i}$ Ice storage charge rate using air-cooled chillers for cooling system i at time t and scenario p, [MW_{th}]

$S^{wc,chs}_{p,t,i}$ Ice storage charge rate using water-cooled chillers for cooling system i at time t and scenario p, [MW_{th}]

$S^{s}_{p,t}$ *Stored thermal energy in ice storage for cooling system i at time t and scenario p,* $[MWh_{th}]$ *Index sets*

i	Cooling system type index set {1, 2, 3} denoted by $\mathscr{I}$
p	Scenario index set {1, 2, 3, 4} denoted by $\mathscr{P}$
s	PV orientation and tracking technology index set {1, 2, 3} denoted by $\mathscr{S}$
t	Time step index set {1, 2, 3, …, 8760} denoted by $\mathscr{T}$

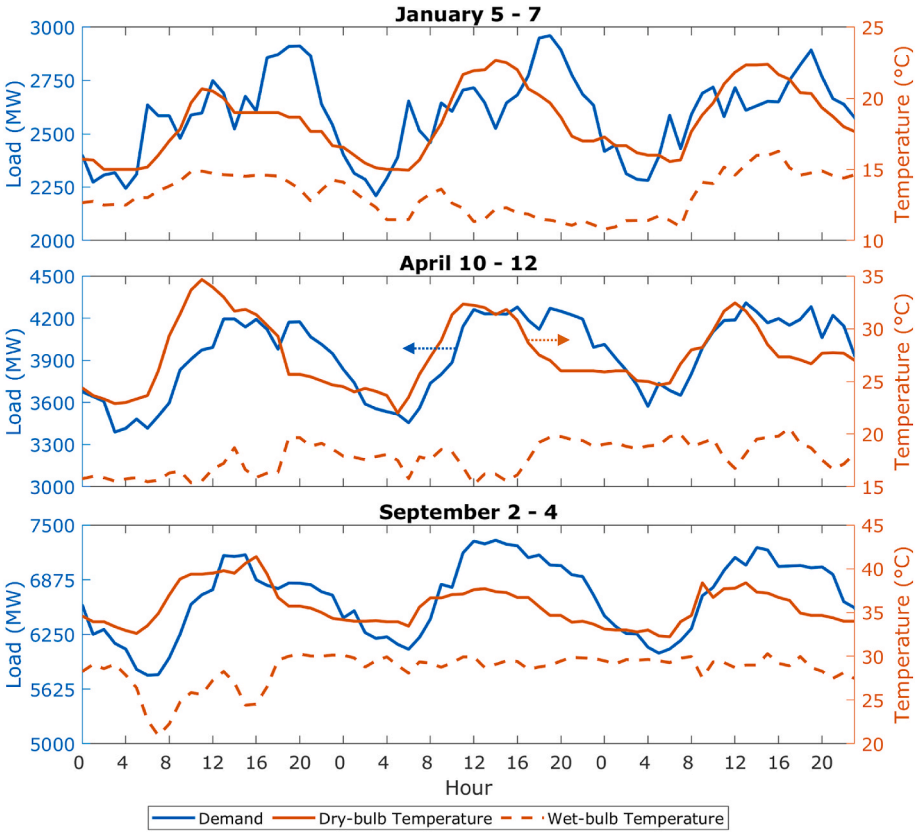

Fig. 1. Qatar's 2016 electricity demand in the winter, spring, and summer for three days on the left y-axis and the ambient conditions, dry and wet-bulb temperatures, on the right y-axis.

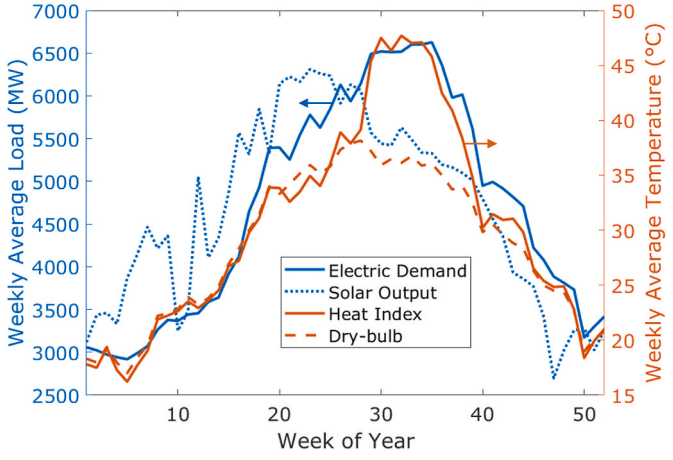

Fig. 2. Qatar 2016 weekly average electric demand and solar output over 19 km^2 in GWh on the left y-axis, and the weekly average heat index in degrees Celsius on the right y-axis. Yearly solar output over 19 km^2 is equivalent to the 2016 electric energy consumption of 42 TWh. Solar output peaks during the summer solstice in June, while electric energy consumption peaks with the heat index in August.

Hour 0 corresponds to midnight (12 a.m.) in all subsequent figures. Daily demand variations are minor relative to seasonal variations driven by high electricity demand from space cooling. In the summer, diurnal demand from space-cooling is synergetic with dry-bulb temperatures, and in the winter, the electricity demand is largely from non-cooling loads. Average daily dry-bulb temperature variations can be as high as 10 $^{\circ}C$ compared to 5 $^{\circ}C$ for wet-bulb temperature.

Threatened by rising sea levels and extreme inhospitable temperatures due to climate change [6], Qatar, alongside the world, must adopt more sustainable approaches to meet increasing energy and cooling demand. While considerations are made for renewable-based energy sources and demand-side management [7–11], which could reduce emissions by 20–25% by 2035, Qatar does not have a net zero or a deep decarbonization plan. However, pathways to decarbonizing the electricity sector in Qatar have been investigated by scholars for large-scale renewables deployment [12–16] and from a distributed building-scale perspective with an emphasis on demand-side management [17–24].

In a comprehensive examination of renewable energy sources in Qatar, Okonkwo et al. [15] explored wind turbines, PV (photovoltaic), concentrated solar power, and biofuels combined with energy storage technologies, including thermal and pump-hydro storage. Okonkwo identified several potential decarbonization pathways with PV and wind generation. However, energy storage systems such as pump hydro were determined to be essential for deep decarbonization, but Qatar's

geography lacks favorable topography. Bohra and Shah [13] and Martinez-Plaza et al. [14] analyzed the long-term potential of solar energy in Qatar. The studies agree on the large potential for grid-scale PV generation. Martinez-Plaza also identified concentrated solar power with large thermal storage as an alternative solution. An investigation of wind turbine potential by Marafia and Ashour [16] reveals promising wind speeds reaching 6.5 m/s at 10 m above ground. The research finds off-shore wind energy suitable for off-grid connection for islands in Qatar and promising for a grid-connected generation. However, unlike solar insolation, wind speed is highly spatially sensitive. Furthermore, meteorological data demonstrate correlated wind speed with intra-annual and diurnal PV generation, which makes wind turbines less able to reduce energy storage needs.

Prior works in the literature identify that the subsidized electricity sector is challenging to decarbonize but affirm Qatar's particular attractiveness for exploiting solar PV. Qatar has a high and predictable solar insolation with a global horizontal irradiance of 2200 kWh/m^2/yr. with few rainy or cloudy days that are synergetic with electricity demand. This is further complemented by access to low-interest capital and abundant suitable land area. Still, demand that continues through the night cannot be met with diurnal solar PV generation without energy storage. Fig. 2 illustrates the synergistic relationship between the 2016 weekly average electric load, solar output, mean heat index, and mean ambient dry-bulb temperature in degrees Celsius. The heat index is a metric for the human perception of the ambient temperature combining the ambient dry-bulb temperature and the humidity level. High humidity between July and September is responsible for the increased electricity demand from space cooling.

In the past, a high fraction of airborne dust hindered large-scale PV deployment in Qatar. However, ongoing research investigates procedures to evaluate and reduce the degradation due to soiling. Abdallah et al. [25] found that fouling can drop panels yield by 15% if not cleaned monthly. A study by Martinez-Plaza et al. [26] determined anti-soiling coating to be ineffective in limiting yield drop but allowed for easier cleaning of the panels. Tahir et al. [27] theoretically analyzed the impact of climate change on mono and bi-facial PV panels in Qatar. The study predicts rising air temp in the years 2050 and 2080 with a reduction in solar insolation by 5–8%. Bi-facial panels are determined to be better suited due to their high energy output and reduced cell temperature. In early 2020, a deal was signed to build an 800 MW solar PV plant in Qatar with a record levelized cost of $15/MWh [28], which was commissioned in October 2022, after this study. Another deal was signed in August 2022 to build two additional solar PV plants with a combined capacity of 875 MW [29].

Individuals' actions to reduce energy consumption or consider alternative energy sources can only have a limited impact on the overall electricity sector's carbon emissions. Any far-reaching impact requires government intervention via direct actions or policy enactments. Carbon pricing is an instrument to increase the cost of generations from carbon-based energy sources to reflect better the environmental damage caused by carbon dioxide emissions. By shifting the burden back to the energy consumers, carbon pricing enables renewable energy to compete with carbon-based energy sources and mobilize investments [30,31]. While there are many forms of carbon pricing, the examined tool is the carbon tax, which adds a cost to gas generation per ton of CO_2 emitted.

This paper examines and analyzes a decarbonization pathway for the electricity sector in Qatar using utility-scale PV generation combined with centralized BESS (Battery Energy Storage System) for electric load shifting and decentralized I-TES (Ice Thermal Energy Storage) for cooling load shifting. In addition to the literature, I-TES is examined as a low-cost means, as opposed to current BESS technologies, to store excess PV generation for subsequent cooling to exploit Qatar's cooling-driven electricity sector. I-TES requires a chiller to produce cooling to convert liquid water into ice. It allows as much as 0.4 MJ/kg of cooling compared to 0.04 MJ/kg for cold water storage since it takes advantage of both the sensible and latent heat from the phase change of liquid water to ice. However, considering I-TES introduces challenges in estimating aggregate thermal cooling demands and systems performance.

This paper solves the planning problem to analyze the impact of the proposed solution on the power grid and to estimate the required capacities, annual system cost, and the achieved percent decarbonization. The problem is formulated in a two-stage stochastic linear program that is solved to minimize overall annual system cost at a given gas price. Like in demand response, I-TES and BESS are strategically dispatched to minimize gas generations use and peak demand. Statistical tools are applied to estimate electric demand due to space cooling from correlations with ambient conditions. The used linear programming tool is extensively employed in utility-scale analyses because it can solve large problems with thousands of continuous and binary variables commonly confronted in large-scale deployment of renewables with energy storage [32–34]. It is also useful for describing cooling systems' aggregate behavior and performance, which tend to exhibit simpler behavior.

In the literature, thermal energy storage has been examined to increase the flexibility of the power grid by responding to the electricity demand and intermittent renewables generations [35–38]. More commonly, in regions with variable electricity rates or demand charges, thermal storage is examined to reduce the required chiller cooling capacity, demand charges, and electricity use charges from load shifting [39–42]. For that mode of operation, the storage is charged during the off-peak period, typically at night, and discharged during the on-peak period, typically in the afternoon, making it suitable for use in schools, offices, and other buildings with dominant diurnal cooling needs. Deetjen et al. [43] considered thermal storage for grid-wide efficiency improvements by taking advantage of the higher cooling efficiency achieved when running chillers at capacity, countering the narrative of thermal storage as net energy consumers. Ruan et al. [39] performed a linear programming analysis to improve the efficiency and economics of building combined cooling, heating, and power using I-TES. They found that gas and electricity charges are the main factors in determining the economic feasibility of I-TES.

The roles and use of BESS in decarbonization are extensively studied [44–52]. Unlike I-TES, BESS can be used to decarbonize all electric loads, but it suffers from capacity degradation, high cost of capacity, and shorter service life. However, the rate at which the cost is falling enables BESS to be cost-competitive with other energy storage technologies [53]. Several studies have stressed the role of utility-scale BESS with PV in reducing carbon emissions and carbon abatement costs compared to PV alone [45–47]. Arbabzadeh et al. [48] examined various energy technologies to reduce the curtailment of variable renewable energy sources and carbon emissions in California and Texas. The results showed that BESSs have a limited role at the current capacity cost. However, a modest decrease in capacity cost can make BESS economically viable.

This paper is organized as follows: the methodology is presented in Section 2. First, the performance of cooling systems as a function of the ambient temperatures is estimated from generic chillers' performance data; second, statistical tools are applied to determine the aggregate cooling load from hourly electric demand; third, the problem formulation is laid out. Section 3 first presents and discusses the cost-optimal system under current cost structures and then examines the role of carbon pricing as a state policy to reduce carbon emissions. Next, a deeply decarbonized system realized with a carbon pricing policy is analyzed in more detail. Last, the impact of declining BESS costs on the cost-optimal system is investigated. The chapter is concluded in Section 4.

2. Methodology

The overall framework utilizes central grid PV and gas generation to distribute electricity via the grid, which can be used for all loads, including BESS charging. The centralized BESS delivers power to the electric grid when needed. I-TES is installed on the customer side as an

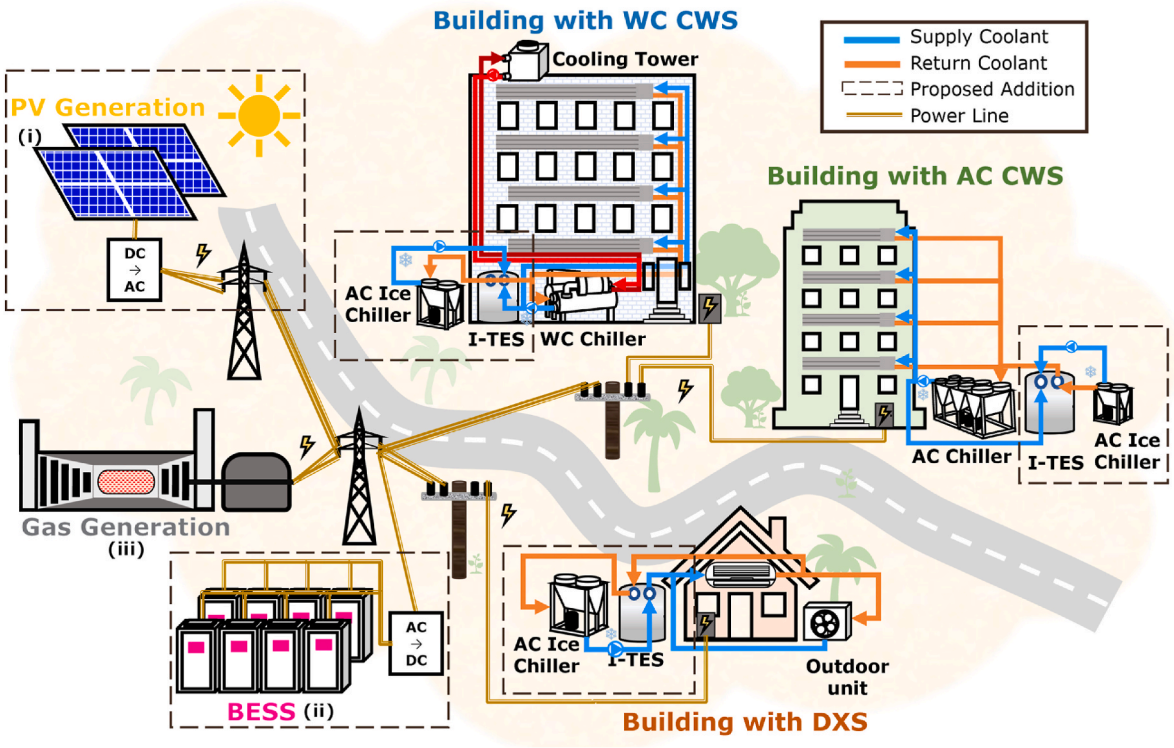

Fig. 3. An illustration of the considered power grid. Central grid PV and gas generation can be used for all loads, including BESS charging. Buildings are classified based on their cooling system type: DXS, AC CWS, and WC CWS. To account for emissions reduction from cooling, the cooling load is assumed to be met in the following order using: (i) PV generation, (ii) BESS, and (iii) gas generation.

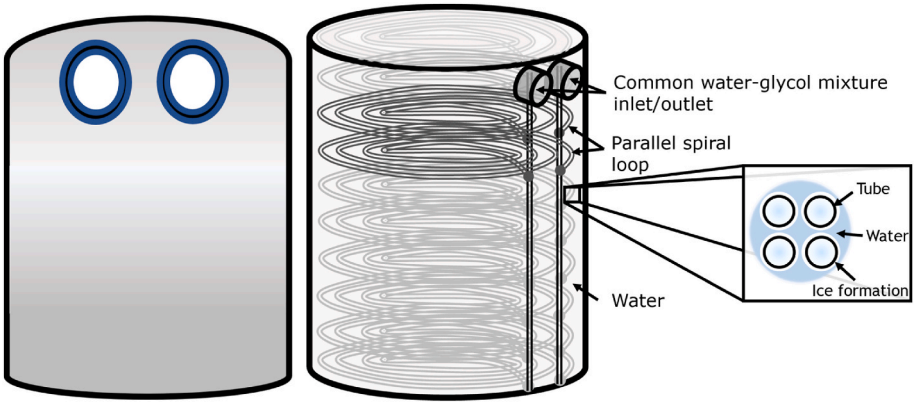

Fig. 4. An illustration of a modular internal-melt I-TES. Multiple parallel spiral circuits are submerged in water inside the tank, and a water-glycol mixture is circulated through the circuits to build and melt the ice around the tubes.

addition to an already existing cooling system and can be charged using existing idle chillers and/or additional ice chillers for a cost. Additional ice chillers are particularly important due to the overlap of PV generation with daytime cooling loads, reducing idle chillers' capacity that could be used for storage charging. Solutions are sought that minimize overall annual system costs from Capex (capital expenditures) and OpEx (operation expenditures) at a given gas price. In accounting for emissions reduction from cooling, the electric cooling load is assumed to be met in the following order using: (i) PV generation, (ii) BESS, and (iii) gas generation.

Cooling systems can be classified into DXS (Direct Expansion System), AC CWS (Air-Cooled Chilled Water System), and WC CWS (Water-Cooled Chilled Water System). DXS, which includes rooftop units, split and ductless mini-split systems, and window units, provides cooling directly from the expansion of the refrigerant. In CWS (Chilled Water System), water is used as an intermediary fluid to transport heat over larger distances and in large buildings. An illustration of the analyzed system is shown in Fig. 3.

I-TES stores thermal energy mainly in the form of latent heat. The are two main types of I-TES: internal and external melt [54]. Internal melt is modularized I-TES with predictable charge and discharge rates and is considered for this study. An illustration of internal melt I-TES is shown in Fig. 4. Inside the tank, multiple parallel loops of tubes are submerged in water. A secondary water-glycol mixture is circulated through the inner loops to freeze or melt the water inside the tank. In external melt I-TES, the entering water comes into direct contact with the ice inside the tank delivering a rapid discharge rate. The higher discharge rate is suitable for specific applications such as providing contingency and high and short-lasting cooling demands. The heat rate of internal melt I-TES is a function of the state of charge and inlet water-glycol mixture

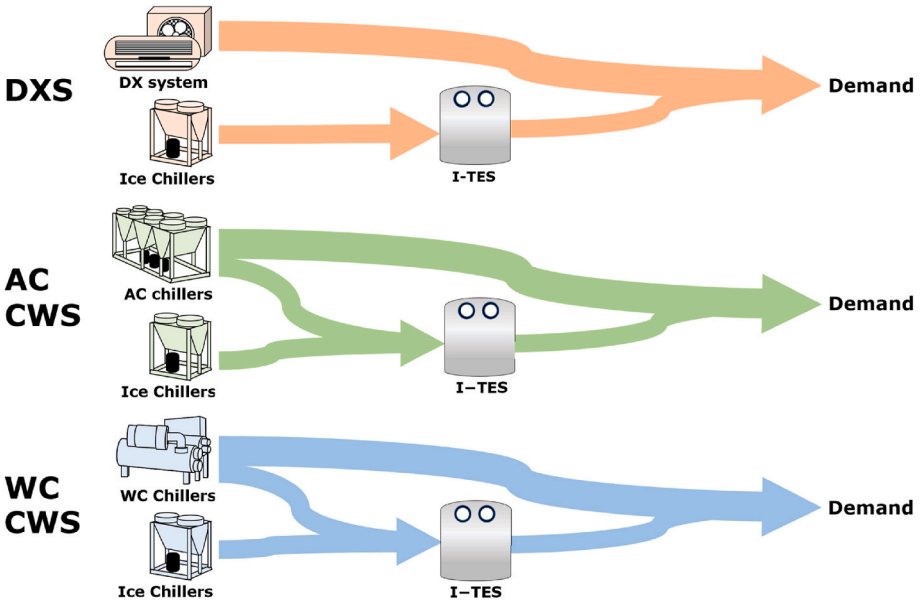

Fig. 5. Pathways to satisfying the cooling demand in the three cooling systems types. While both AC and WC CWS are capable of ice-making, additional AC ice chillers can be installed at a cost. Additional ice chillers must be installed with the I-TES for the DXS.

temperature and flowrate [55,56]. The charge rate is highest during the sensible charging stage due to a greater temperature difference between the entering water-glycol mixture and the average tank water temperature. Once the tank is brought to freezing temperature, the charge rate reduces as the thermal resistance increases due to ice formations. Similarly, discharging of I-TES is initially higher when the water in the tank is completely frozen. The discharge rate reduces as the ice around the tube melts.

DXS and AC CWS are AC (Air-Cooled) systems, and their COP (Coefficient of Performance) is associated with the ambient dry-bulb temperature. WC CWS utilizes WC (Water-Cooled) condensers, and their COP is associated with the wet-bulb temperature as heat is ultimately rejected using evaporative cooling in a cooling tower. WC systems run more efficiently, benefiting from lower condensing temperatures, especially in dry seasons. The current approach to meet the cooling demand in Qatar, which lacks thermal storage, uses a mix of DXS, AC CWS, and WC CWS. The considered pathway of load shifting using I-TES for each cooling system type is illustrated in Fig. 5 below.

The DXS′ I-TES can only be charged using additionally installed ice chillers as currently installed standard systems are incompatible with ice-making. For AC and WC CWS, I-TES can be charged using idle and additionally installed chillers capacities. All additional ice chillers are lower-cost AC chillers, provided they utilize low-cost excess generation for I-TES charging.

The analysis is performed with four scenarios, each with one year of hourly solar insolation, electric demand, and meteorological data, from 2013 to 2016. However, as the demand has been growing yearly, the demands from 2013 to 2015 are normalized to the peak demand of 2016. The aggregate cooling load is determined using the normalized hourly electric demand and its respective year's meteorological data set (Doha International Airport weather station). The 2016 scenario was taken as the reference scenario in all produced figures.

2.1. Cooling system COP estimation

The COP of cooling systems is affected by the refrigerant condensing temperatures influenced by the ambient conditions. The dry-bulb temperature influences AC systems' condensing temperature as they depend on dry cooling to reject heat to the ambient. The wet-bulb temperature influences the condensing temperature of WC systems as they rely on evaporative cooling. The fundamentally lower wet-bulb temperature reduces the condensing temperature and improves system performance.

The COP of AC and WC systems as a function of ambient conditions is derived from the behavior of generic system performance analogous to Deetjen et al. work [43,58]. Although less significant, the performance of cooling systems is also a function of their loading. Chillers' performance data are taken from the library of chillers in EnergyPlus at the typical design water supply temperature of 7 $^{\circ}C$ and the optimal part-load ratio of 80%. The performance data are extracted and used with Gordon-Ng's model to predict chiller performance across a broader range of ambient temperatures than permitted by the DOE-2 model used by EnergyPlus. Details of the methodology used are explained in another work in Ref. [59].

Two AC chillers with typical performance are selected: Carrier 19XA and McQuay AGZ, and two WC chillers: Trane RTHB and Carrier 19XR. Auxiliary equipment, such as water pumps and tower fans, consumes on the order of 10% of total system energy in AC CWS and about 20% in WC CWS [60]. The entering condenser temperature for WC CWS is taken at a standard 3 $^{\circ}C$ above the wet-bulb temperature. A power curve is fitted to the estimated system COP for AC systems in refrigeration and ice-making (I-TES charging) mode, which are given by:

$$COP^{ac}_{p,t} = 14.44\left(T^{db}_{p,t}\right)^{-0.5}, [^{\circ}C] \quad \left(T^{db}_{p,t} > 0^{\circ}C\right) \tag{1}$$

$$COP^{ac,ice}_{p,t} = COP^{ac}_{p,t} \times \varphi^{ice}, [^{\circ}C]\left(T^{db}_{p,t} > 0^{\circ}C\right) \tag{2}$$

and for WC systems:

$$COP^{wc}_{p,t} = 25.25\left(T^{wb}_{p,t}\right)^{-0.56}, [^{\circ}C]\left(T^{wb}_{p,t} > 0^{\circ}C\right) \tag{3}$$

$$COP^{wc,ice}_{p,t} = COP^{wc}_{p,t} \times \varphi^{ice}, [^{\circ}C]\left(T^{wb}_{p,t} > 0^{\circ}C\right) \tag{4}$$

where the subscripts p is the scenario index set $\{1,2,3,4\}$ denoted by $\mathscr{P}$ and refers to years 2013–2016, and t is the time step index set $\{1,2,3,\ldots,8760\}$ denoted by $\mathscr{T}$ that refers to the hour of the year, φ^{ice} is the depressed chiller performance factor in ice-making mode and is about 0.8, and $T^{db}_{p,t}$ and $T^{wb}_{p,t}$ are the dry and wet-bulb temperatures, respectively, in degrees celsius. Running the chillers in ice-making mode reduces the COP due to decreased refrigerant vapor quality in the

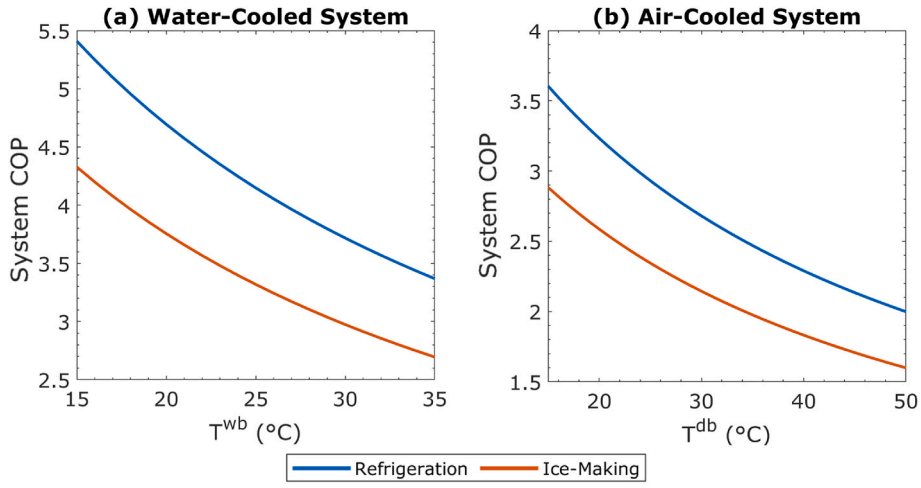

Fig. 6. System COP for (a) WC systems v. wet-bulb temperature and (b) AC CWS v. dry-bulb temperature in refrigeration and ice-making modes. AC systems include AC CWS and DXS.

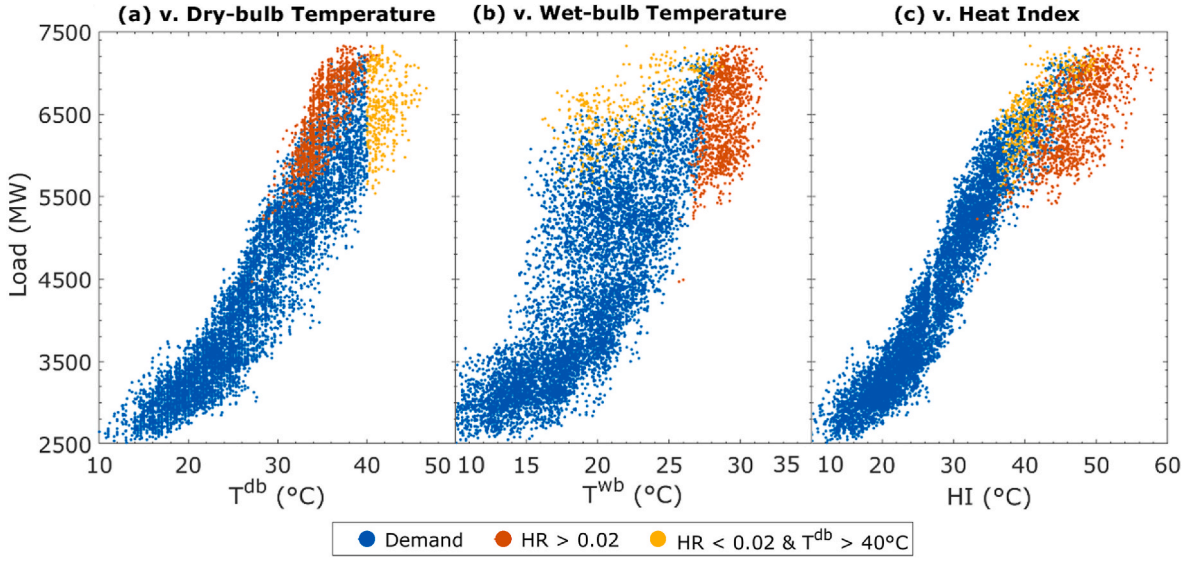

Fig. 7. Qatar's 2016 electric demand vs. (a) dry-bulb temperature, (b) wet-bulb temperature, and (c) heat index. Data points highlighted in red are warm and humid hours with a humidity ratio ($HR_{p,t}$) $\geq$ 0.02, and in yellow are warm and dry hours with $HR_{p,t} \leq 0.02$ and $T^{db}_{p,t} \geq 40\ ^{\circ}C$.

evaporator [61–63]. Fig. 6 visualizes the developed relation between system COP and the wet-bulb temperature for WC systems and dry-bulb temperatures for the AC systems in refrigeration and ice-making mode.

An exponential improvement in COP is realized with reduced temperatures. Design system COP, which dictates the installed nominal cooling capacities and performance, for WC systems of 4.2 is evaluated at the standard design wet-bulb temperature of 25 $^{\circ}C$, and for the AC system of 2.4 is evaluated at the standard design dry-bulb temperature of 35 $^{\circ}C$ in refrigeration mode. The developed COP relation allows for the conversion between electric and thermal loads necessary for thermal energy storage analysis.

Ambient conditions also impact the cooling capacity of cooling systems. The capacity of a cooling system in refrigeration mode is associated with the COP. In ice-making mode, the cooling capacity is associated with both the COP and the depressed chiller capacity factor, ψ^{ice}. The factor accounts for the loss in refrigerant thermal capacity in the evaporator due to reduced refrigerant vapor saturation density relative to refrigeration mode and is about 0.75. Running the chillers in ice-making mode can depress their cooling capacity by 30–40% relative to their nominal capacities [64]. For AC chillers, the cooling capacity relation for both modes is given by:

$$C^{AC} \propto COP^{ac}_{p,t} (\text{Refrigeration mode}) \quad (5)$$

$$C^{AC,ice} \propto COP^{ac,ice}_{p,t} \psi^{ice} \ (\text{Ice} - \text{making mode}) \quad (6)$$

and for WC chillers:

$$C^{WC} \propto COP^{wc}_{p,t} (\text{Refrigeration mode}) \quad (7)$$

$$C^{WC,ice} \propto COP^{wc,ice}_{p,t} \psi^{ice} (\text{Ice} - \text{making mode}) \quad (8)$$

2.2. Cooling load estimation

Qatar's electric demand varies with meteorological conditions and the time of day, influenced by daily social routines and building occupancy. There are several methods to estimate the aggregate electric demand from space cooling. The methods can be classified into bottom-up and top-down approaches [65]. In the bottom-up approach, simulation tools are used to predict the cooling demand of building stock; they

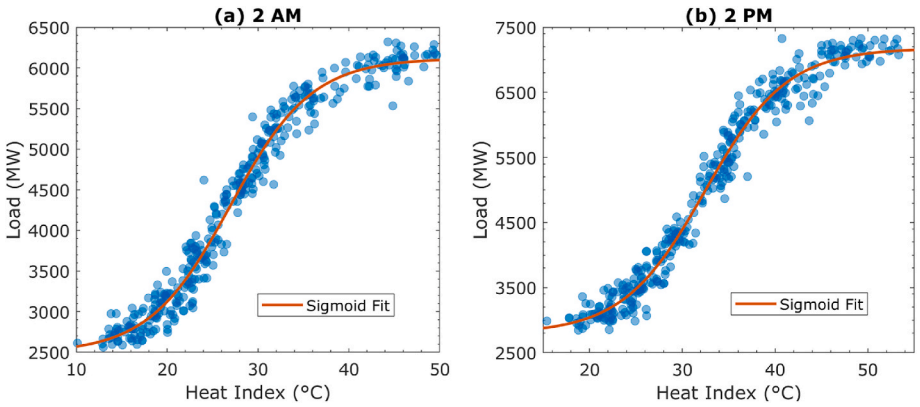

Fig. 8. 2016 Electric demand v. heat index at (a) 2 a.m. and (b) 2 p.m. A sigmoid function is fitted with 4 data points: peak and base demand, growth factor, and heat index mid-point.

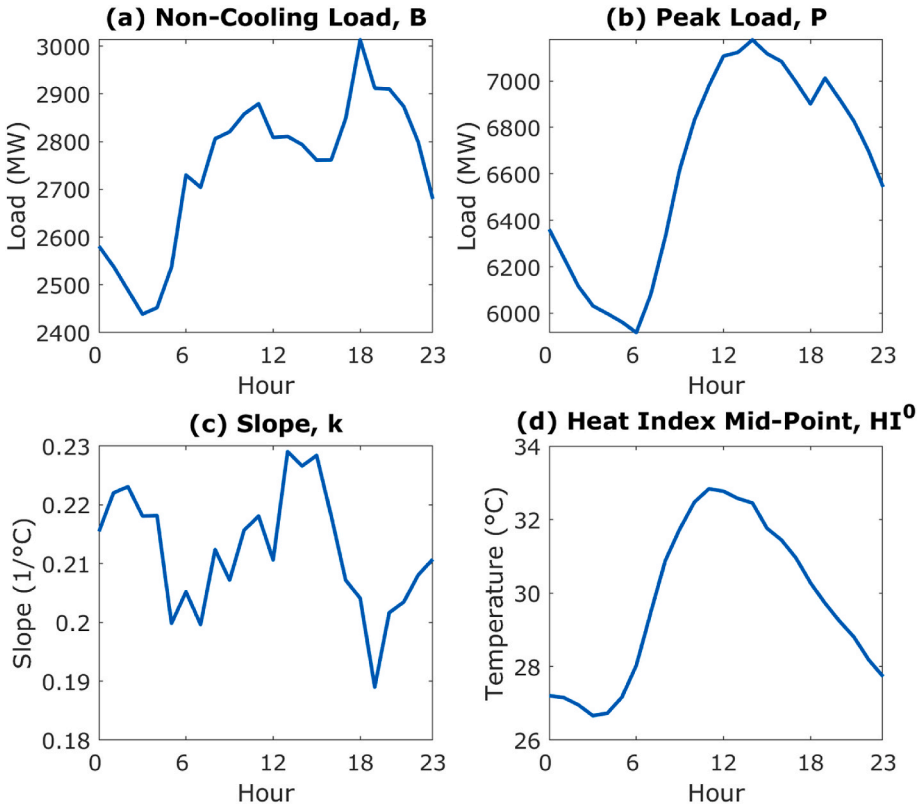

Fig. 9. The four fitted parameters: (a) base load $B_{p,t}$, (b) peak demand $P_{p,t}$, (c) slope $k_{p,t}$, and (d) heat index midpoint $HI^0_{p,t}$ at the hour of the day for the 2016 scenario.

require knowledge of buildings construction, orientation, and use and are computationally demanding. Statistical analysis aggregates the estimated cooling demand for the entire building stock. In top-down approaches, statistical methods are used to isolate demand from space cooling from the total electric demand. A way to isolate the cooling load is by subtracting the total electric demand from the base load (days with no cooling needs). This method assumes that all intra-annual variations in electric demand from the reference base load are due to space cooling. Bayram et al. [4] employed this method to estimate Qatar's cooling load. Another top-down approach estimates the electric demand based on correlation with meteorological parameters, such as linear regression of demand with ambient temperature. This method was used by Saffouri et al. [3] to estimate Qatar's cooling load, which produced a similar estimate to the former approach used by Bayram.

A slightly more sophisticated method is considered in this work. The cooling load is estimated as the change in electric demand due to the change in ambient conditions at every hour of the day using least-squares regression. In Qatar, the time of the day and ambient conditions are found to be excellent predictors of electric demand. In contrast, the wind speed was poorly correlated with electric demand, with a correlation coefficient of 4%. Furthermore, the day of the week had an insignificant effect on the estimated cooling load and was not considered. Three ambient conditions metrics were examined: dry-bulb temperature, wet-bulb temperature, and heat index. The heat index, which is the human perception of ambient conditions, was found to be a better indicator of electricity demand, with a correlation coefficient of 96% compared to 93% with dry-bulb temperature and 83% with wet-bulb temperature. A plot of the metrics against the electric demand is in Fig. 7.

The use of dry-bulb temperature as a metric underpredicts the load

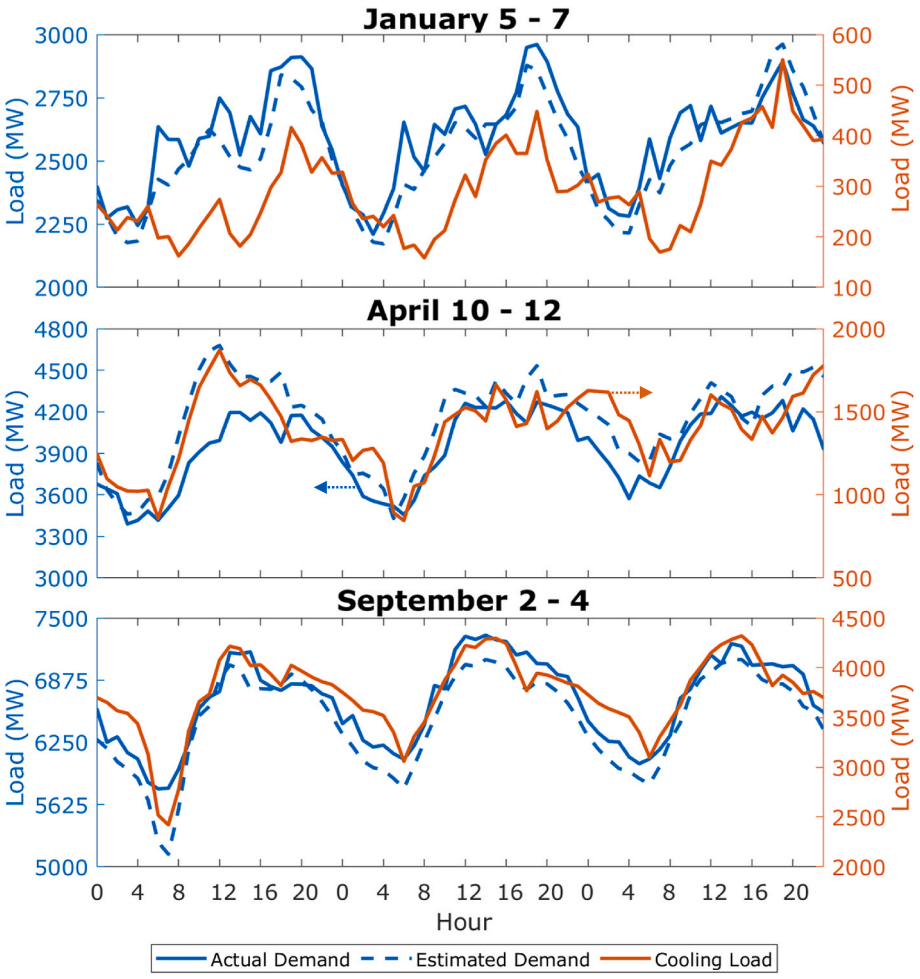

Fig. 10. Actual electric load, $\mathscr{D}_{p,t}$, estimated electric load, $B_{p,t} + \mathscr{D}^{\mathscr{C}}_{p,t}$ on the left y-axis and electric cooling load, $\mathscr{D}^{\mathscr{C}}_{p,t}$, on the right y-axis from the logistic curve regression for the 2016 scenario. The estimated load generally agrees with the actual load, with an average percent difference of 3.5%.

Table 1
Characteristics parameters in the model.

Item	Parameter	Symbol	Value
PV	Inverter efficiency	η^{I}	98%
BESS	Initially charge	$\mathscr{B}^{s}_{p,t=0}$	100%
	Charge efficiency	$\eta^{BESS,chs}$	92%
	Discharge efficiency	$\eta^{BESS,dis}$	92%
	Self-discharge efficiency	$\eta^{BESS,sdis}$	99.9%
I-TES	Charge capacity	$f^{ITES,chs}$	1/6 hr^{-1}
	Discharge capacity	$f^{ITES,dis}$	1/3 hr^{-1}
	Initially charge	$S^{s}_{p,t=0,i}$	100%
	Self-discharge efficiency	$\eta^{ITES,sdis}$	99.9%
Chiller	Existing DXS cooling capacity	$C^{DX,des}$	3100 MW_{th}
	Existing AC CWS cooling capacity	$C^{AC,des}$	6100 MW_{th}
	Existing WC CWS cooling capacity	$C^{WC,des}$	5700 MW_{th}
	Depressed chiller capacity factor	ψ^{ice}	0.75
	Design WC systems COP	$COP^{wc,des}$	4.2
	Designed AC systems COP	$COP^{ac,des}$	2.4

Table 2
Financial parameters in the model.

Item	Unit	Expense	Symbol	Value
PV	Fixed-tilt	Capex	$c^{PV,C}_{1}$	\$450/$kW_{p,dc}$
		OpEx	$c^{PV,O}_{1}$	\$10/$kW_{p,dc}$/yr
	Single-axis tracking	Capex	$c^{PV,C}_{2}$	\$550/$kW_{p,dc}$
		OpEx	$c^{PV,O}_{2}$	\$15/$kW_{p,dc}$/yr
	Dual-axis tracking	Capex	$c^{PV,C}_{3}$	\$700/$kW_{p,dc}$
		OpEx	$c^{PV,O}_{3}$	\$20/$kW_{p,dc}$/yr
I-TES	Internal melt	Capex	c^{ITES}	\$14/kWh_{th} (\$50/TR-hr)
BESS	4-h Li-ion	Capex	c^{BESS}	\$250/kWh
Chiller	Ice chillers for I-TES charging	Capex	$c^{IceChl,C}$	\$57/kW_{th} (\$200/TR)
		OpEx	$c^{IceChl,O}$	\$3/kW_{th}/yr. (\$20/TR)
Misc.	Gas generation cost	OpEx	c^{GT}	\$37/MWh
	Gas price	OpEx	–	\$3.33/MMBtu
	Capital	Interest rate	ir	3.5%
		Service life	yr	25 years
		BESS service life	yrb	10 years
	Peak gas generation cost	OpEx	c^{PGT}	\$5/MW_{p}

on warm and humid days with a humidity ratio ($HR_{p,t}$) greater than 0.02 in July–August, whereas the use of wet-bulb temperatures underpredicts the load on dry and warm days ($HR_{p,t} < 0.02$ and $T^{db}_{p,t} > 40°C$) in June–July. On the other hand, using the heat index well-predicted the demand under both dry and humid conditions. This can be observed with higher electric demands associated with a higher heat index compared to lower dry and wet-bulb temperatures. The higher prediction power is attributed to the compounding effect of humidity level and dry-bulb temperature on the heat index, which drives cooling loads.

A logistic growth curve is fitted to the exhibited sigmoid relation

Table 3
Cost-optimal system under the current cost structure.

Parameter	Value	Notes
Solar PV capacity	8.1 $GW_{p,dc}$	5.9 $GW_{p,dc}$ fixed-tilt 2.2 $GW_{p,dc}$ single-axis tracking
I-TES thermal capacity	28 GWh_{th}	3 GWh_{th} DXS 15 GWh_{th} AC CWS 10 GWh_{th} WC CWS
Additional ice chiller capacity	0.7 GW_{th}	DXS
Peak gas generation demand	6.0 GW	Across all scenarios

Table 4
Cost-optimal system characteristics averaged over the four scenarios under the current costs structure.

Parameter	Value	Notes
Cost	$1239 million/yr.	Annual cost from Capex and OpEx
Average power generation cost	$29/MWh	From gas and PV generation
Demand met by gas generation	57%	–
Demand met by PV generation	38%	Directly
Electric load shifted by I-TES	5%	All cooling systems
Cooling demand met by PV generation	41%	Directly
Cooling demand met by I-TES	13%	All cooling systems
Solar capacity factor	25%	After curtailment
Curtailment	10%	Of total PV generation
I-TES average charge residency	17 h	Based on first-in, first-out
I-TES average capacity utilization	70%	Equivalent full cycles per day

between electricity demand and the heat index; two example hours (2 a.m. and 2 p.m.) are shown in Fig. 8. The aggregate electric cooling load from sigmoid function is as follows:

$$\mathscr{D}^{\mathscr{C}}_{p,t} = \frac{P_{p,t} - B_{p,t}}{1 + e^{-k_{p,t}\left(HI - HI^{0}_{p,t}\right)}} \tag{9}$$

where $k_{p,t}$ is the slope, $B_{p,t}$ is the non-cooling load, $P_{p,t}$ is the peak load, and $HI^{0}_{p,t}$ is the heat index midpoint, all shown in Fig. 9 at each hour. $B_{p,t}$ peaks in the evening and troughs in the morning suggestive of correlation with buildings occupancy; $P_{p,t}$ peaks midday and is driven by cooling needs; $k_{p,t}$ is the slope (curve's steepness) and is time-insensitive; $HI^{0}_{p,t}$ is influenced by the yearly temperature range at every hour of the day. The non-cooling portion of the electric demand is determined by deducting the estimated electric cooling load, $\mathscr{D}^{\mathscr{C}}_{p,t}$, from the total electric demand, $\mathscr{D}_{p,t}$, as follows:

$$\mathscr{D}^{\mathscr{N}}_{p,t} = \mathscr{D}_{p,t} - \mathscr{D}^{\mathscr{C}}_{p,t} \tag{10}$$

Ambient conditions insensitive cooling demand in large buildings such as malls and airports cannot be distinguished from the non-cooling baseload using statistical methods and thus was not unaccounted for in the cooling load. This method estimates that space cooling in Qatar was responsible for 42% of electric demand in 2016, slightly higher than Saffouri et al. [3] and Bayram et al. [4] estimate of approximately 35%. The difference is credited to a more accurate estimate of the cooling load in the low cooling periods. The estimated aggregate thermal cooling demand is divided proportionally to the maximum aggregate electric load from DXS, AC CWS, and WC CWS and is converted to thermal cooling demand using the developed COP relation as follow:

$$\mathscr{C}^{DX}_{p,t} = \frac{\mathscr{D}^{\mathscr{C}}_{p,t}}{\max\limits_{p\in\mathscr{P},t\in\mathscr{T}}\left[\mathscr{D}^{\mathscr{C}}_{p,t}\right]} E^{DX}\, COP^{ac}_{p,t} \tag{11}$$

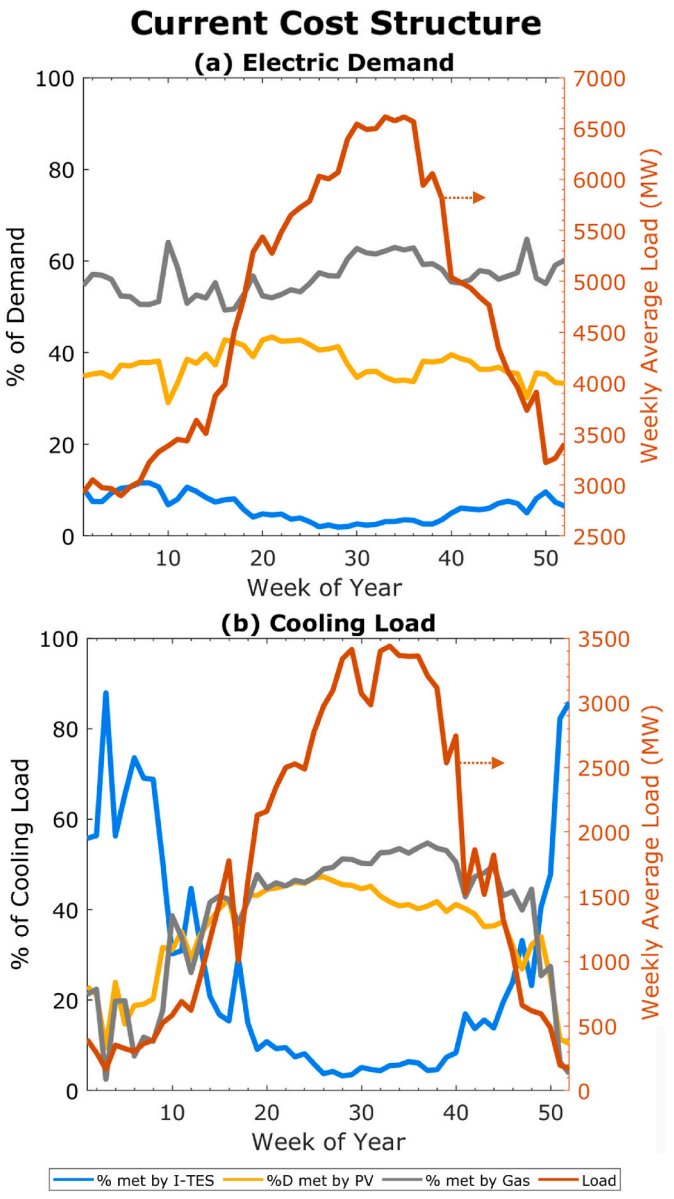

Fig. 11. 2016 scenario cost-optimal system under current cost structure with a breakdown of contribution to supplying (a) electric demand and (b) electric cooling load with percent load shifted by I-TES (% met by I-TES), directly met by PV (%D met by PV), and met by gas (% met by Gas) on the left y-axis and the average weekly load on the right y-axis.

$$\mathscr{C}^{AC}_{p,t} = \frac{\mathscr{D}^{\mathscr{C}}_{p,t}}{\max\limits_{p\in\mathscr{P},t\in\mathscr{T}}\left[\mathscr{D}^{\mathscr{C}}_{p,t}\right]} E^{AC}\, COP^{ac}_{p,t} \tag{12}$$

$$\mathscr{C}^{WC}_{p,t} = \frac{\mathscr{D}^{\mathscr{C}}_{p,t}}{\max\limits_{p\in\mathscr{P},t\in\mathscr{T}}\left[\mathscr{D}^{\mathscr{C}}_{p,t}\right]} E^{WC}\, COP^{wc}_{p,t} \tag{13}$$

where E^{DX}, E^{AC}, and E^{WC} are the maximum electric load of existing DXS, AC CWS, and WC CWS, respectively. As reported by the utility, the maximum electric loads from AC CWS and WC CWS are 2 and 1.1 GW, respectively [66]. DXS is responsible for the remaining cooling loads with an estimated maximum aggregate electric load of 1.3 GW. The electric cooling load is converted to thermal cooling demand using the developed COP relation. Because of data deficiency, it is reasonably assumed that the three cooling systems are similarly represented in

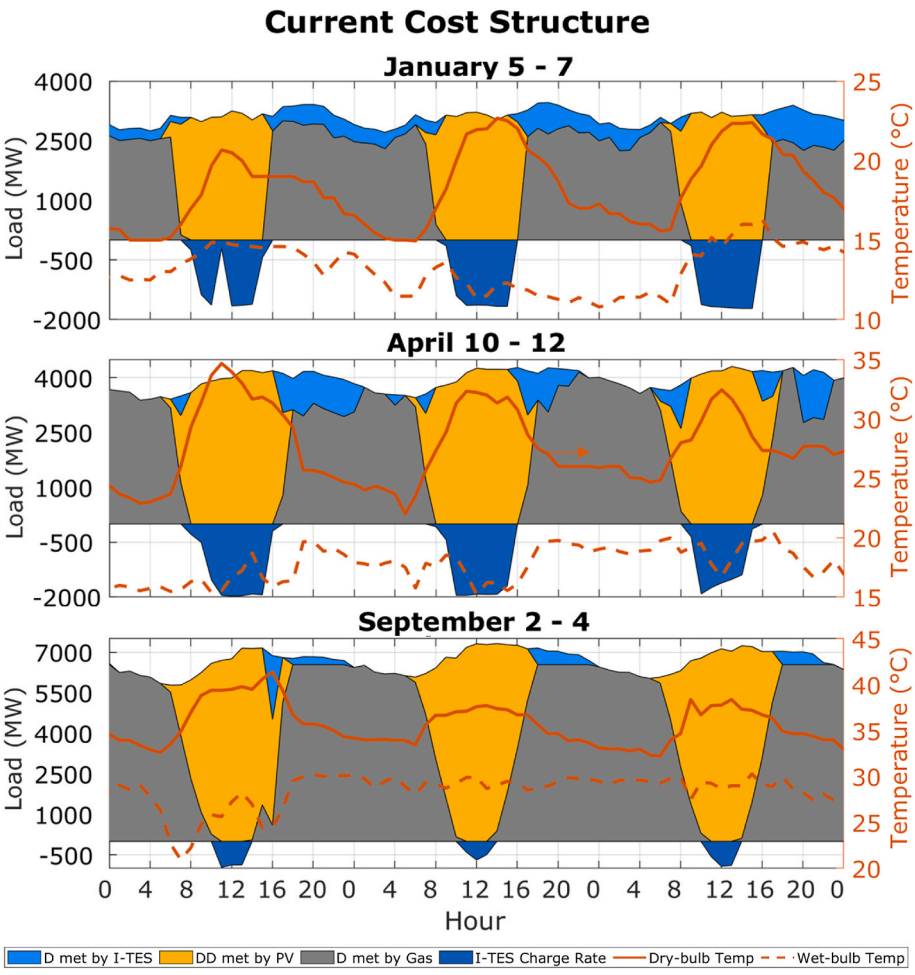

Fig. 12. Cost-optimal system hourly load profile with D (demand) met by I-TES, DD (demand directly) met from PV, D (demand) met by gas, and on the left y-axis and the ambient temperatures on the right y-axis for three days in winter, spring, and summer. I-TES charge rate is shown in negative.

different sectors. It should be noted that WC and AC cooling systems' electric loads are unlikely to be perfectly correlated, as the estimated aggregate cooling demand suggests, since their performance is affected by two different atmospheric parameters: the wet and dry-bulb temperatures. Nevertheless, the ambient dry-bulb and wet-bulb temperatures are generally well-correlated with correlation coefficients of 0.72, 0.81, and 0.85 for average hourly, daily, and weekly temperatures, respectively, which are unlikely to produce significant errors.

The electric demand, $\mathscr{D}_{p,t}$, estimated electric demand from non-cooling and cooling loads, $B_{p,t} + \mathscr{D}^{\mathscr{C}}_{p,t}$, and the hourly estimated aggregate cooling load, $\mathscr{D}^{\mathscr{C}}_{p,t}$, are shown in Fig. 10 for three consecutive days in winter, spring, and summer. The estimated demand generally agrees with the actual electric demand with an average percent difference of 3.5%. In the warmer seasons, the cooling load peaks in the afternoon between 11 a.m. and 3 p.m., and troughs in the early morning between 3 and 6 a.m., as expected, are well-correlated with the electric demand and ambient heat index. During the peak cooling demand season, the contribution to electric load from space cooling can be as high as two-thirds of the electric demand. In the winter, counter to expected trends, there is a higher cooling load in the evening, mostly attributed to higher building occupancy and cooling footprint.

2.3. Problem formulation

The problem is modeled in a two-stage stochastic linear programming that minimizes the expected annual system cost across four scenarios of demand, ambient dry and wet-bulb temperatures, and solar insolation. The intention is to account for annual variations in the ambient conditions, which influence the cooling demand and PV power output. The first stage decision variables are the installed capacities, and the second stage decision variable is the consumed gas. The objective function that is to be minimized is as follows:

$$\begin{aligned} min\ Cost = & \left(\sum_{s \in \mathscr{S}} c_s^{PV,C} C_s^{PV} + \sum_{i \in \mathscr{I}} \left[c^{ITES} C_i^{ITES} + c^{IceChl,C} C_i^{IceChl} \right] \right) \frac{ir(ir+1)^{yr}}{(1+ir)^{yr}-1} \\ & + c^{BESS} C^{BESS} \frac{ir(ir+1)^{yrb}}{(1+ir)^{yrb}-1} + \sum_{s \in \mathscr{S}} c_s^{PV,O} C_s^{PV} \\ & + \sum_{i \in \mathscr{I}} \left[c^{IceChl,O} C_i^{IceChl} \right] + \mathbb{E}_{p \in \mathscr{P}} \left[c^{GT} \sum_{t \in \mathscr{T}} GT_{p,t} \right] \\ & + c^{PGT} GT^{P} \end{aligned} \tag{14}$$

The objective function contains the annualized Capex and associated annual OpEx from installed capacities of PV, I-TES, BESS, and additional ice chillers and the expected annual OpEx of existing gas generation from gas use. The subscript i is the cooling system technology index set {1, 2, 3} denoted by $\mathscr{I}$ that corresponds to 1) DXS, 2) AC CWS, and 3) WC CWS, s is PV orientation and tracking technology index set {1, 2, 3} denoted by $\mathscr{S}$ that corresponds to 1) optimal fixed-tilt angle at Qatar latitude of 25 ° [67], 2) single-axis tracking, and 3) dual-axis tracking PV systems. C_s^{PV}, C_i^{ITES}, C_i^{IceChl}, and C^{BESS} are installed capacities of PV, I-TES, ice chillers, and BESS, respectively. $c_s^{PV,C}$ and $c_s^{PV,O}$ are installed PV Capex and OpEx. $c^{IceChl,C}$ and $c^{IceChl,O}$ are installed ice chillers Capex and OpEx.

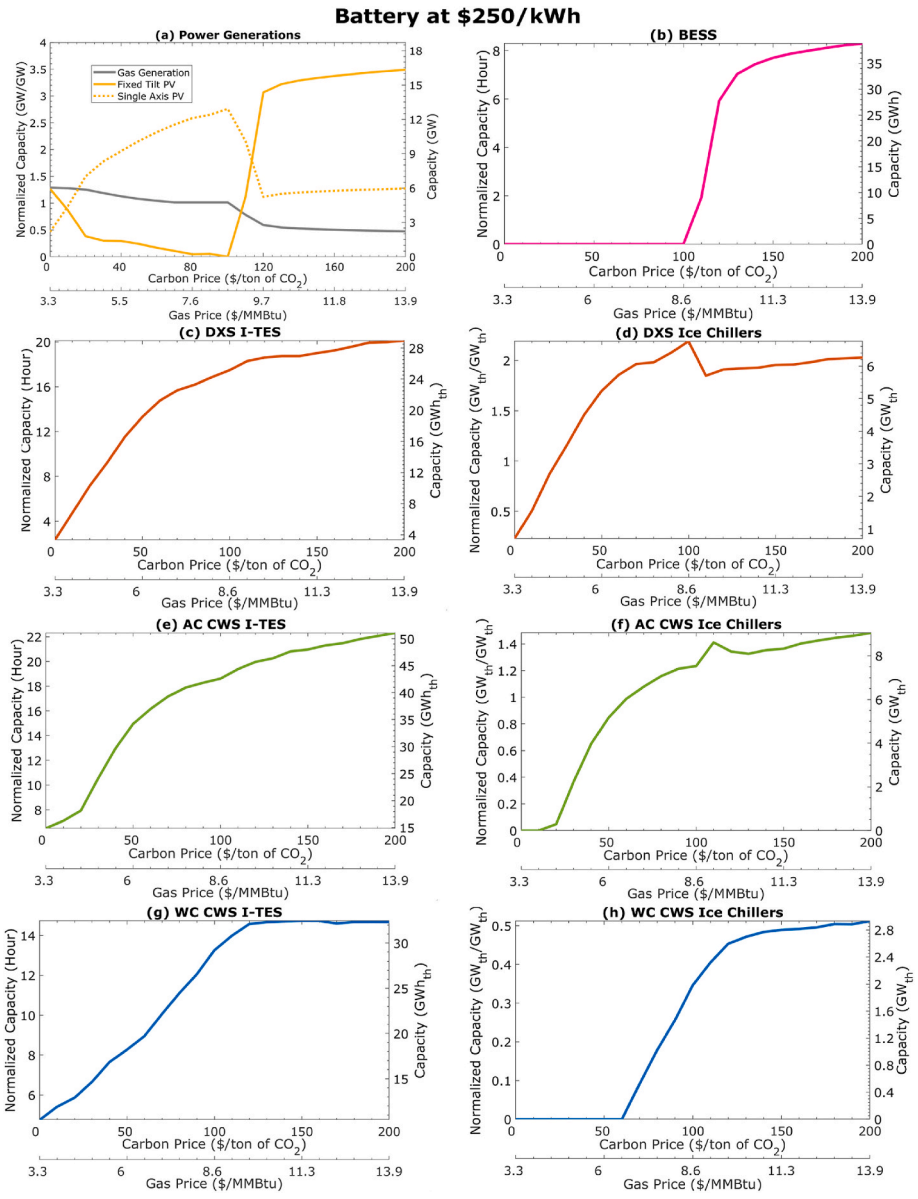

Fig. 13. Cost-optimal system as carbon price increases. Power generation and BESS capacities are normalized to the 2016 yearly average electric demand of 4.7 GW. I-TES capacity is normalized to the average aggregate cooling demand of 1.4 GW_{th} for DXS, 2.3 GW_{th} for AC CWS, and 2.2 GW_{th} for WC CWS. Ice chiller capacity is normalized to the aggregate cooling system capacity of 3.1 GW_{th} for DXS, 6.1 GW_{th} for AC CWS, and 5.7 GW_{th} for WC CWS.

c^{ITES} and c^{BESS} are the installed I-TES and BESS Capex, respectively. *ir* is the interest rate, *yr* is the service life for PV, I-TES, and ice chillers, and *yrb* is the BESS service life. c^{GT} is the average cost of produced energy using gas-fired generation, $GT_{t,p}$ is power supplied by gas generation, and GT^{P} is peak gas generation demand. c^{PGT} is a small cost ($5/$MW_p$) assigned to the peak gas generation demand to find a unique solution that minimizes peak gas generation demand without impacting the cost-optimal system. The term $\mathbb{E}_{p\in\mathscr{P}}\left[c^{GT}\sum_{t\in\mathscr{T}} GT_{p,t}\right]$ is the expected annual cost from gas use across 4 scenarios (2012–2016), each with an assumed equal likelihood of occurrence (25%).

The first constraint balances the supply and demand of power in the electricity grid as follows:

$$GT_{p,t} + \mathscr{B}^{dis}_{p,t} - \mathscr{B}^{chs}_{p,t} + \eta^{I}\sum_{s\in\mathscr{S}} I_{p,t,s}C^{PV}_{s} - PV^{curt}_{p,t} = \mathscr{D}^{\mathscr{N}}_{p,t} + \mathscr{D}^{DX}_{p,t} + \mathscr{D}^{AC}_{p,t} + \mathscr{D}^{WC}_{p,t}, \forall p \in \mathscr{P}, \forall t \in \mathscr{T} \quad (15)$$

The right-hand side of the equation is the electric demand, which comprises the non-cooling, $\mathscr{D}^{\mathscr{N}}_{p,t}$, and the aggregate electric cooling loads: $\mathscr{D}^{DX}_{p,t}$ from the DXS, $\mathscr{D}^{AC}_{p,t}$ from AC CWS, and $\mathscr{D}^{WC}_{p,t}$ from WC CWS. $\mathscr{B}^{dis}_{p,t}$ is the dispatched power from BESS, and $\mathscr{B}^{chs}_{p,t}$ is the BESS charging rate. $I_{p,t,j}$ is solar insolation normalized by peak sun hour, and η^{I} is the inverter efficiency. The terms $\eta^{I}\sum_{s\in\mathscr{S}} I_{p,t,s}C^{PV}_{s}$ and $PV^{curt}_{p,t}$ are the supplied and curtailed power from PV generation, respectively. Only excess PV generation can be used for energy storage charging in a cost-optimal system, and other uses are sub-optimal due to the performance loss associated with the charging and dispatch processes. Gas-fired generations were modeled as a single equivalent power generation plant, and minimum part load and up/down times for the individual generation were not considered. Since gas-fired generations can ramp up to capacity in less than an hour and the analysis was done hourly, ramping constraints were disregarded. Peak gas generation demand in all scenarios is captured in the following constraint and penalized by the objective function:

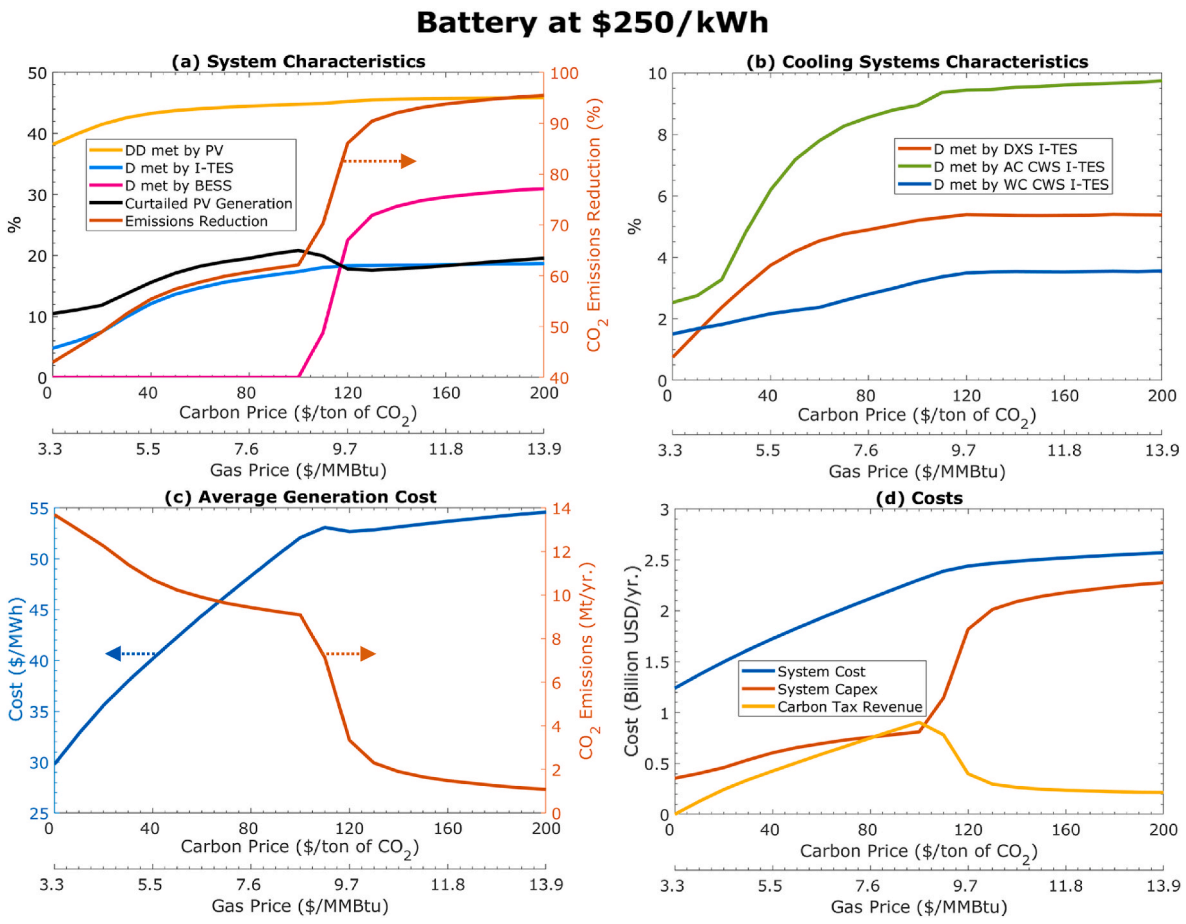

Fig. 14. As carbon price increases: (a) overall system characteristics, (b) cooling system characteristics, (c) average generation cost and total CO_2 emissions, and (d) system's annual cost, Capex, and revenue from the carbon tax (carbon pricing).

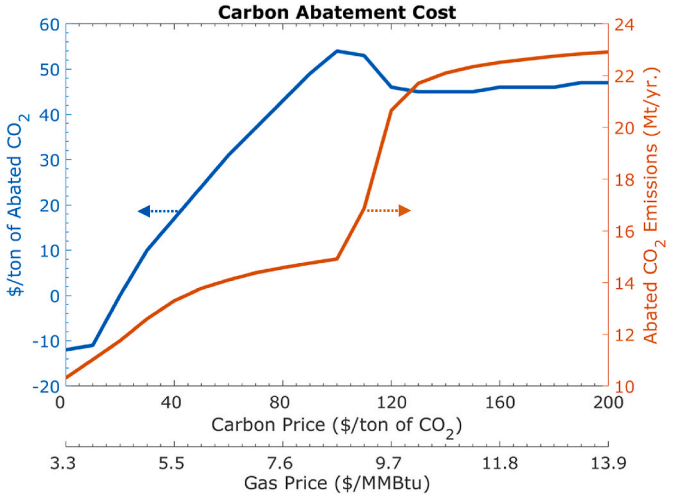

Fig. 15. As carbon price increases, carbon abatement costs on the left y-axis and abated CO_2 emissions on the right y-axis, relative to the current system of all gas-based generations.

Table 5
Cost-optimal system at $140/ton of CO_2 carbon price.

Parameter	Value	Notes
Solar PV capacity	21 $GW_{p,dc}$	15 $GW_{p,dc}$ fixed-tilt 6 $GW_{p,dc}$ single-axis tracking
I-TES capacity	107 GWh_{th}	27 GWh_{th} DXS 48 GWh_{th} AC CWS 32 GWh_{th} WC CWS
Additional ice chiller capacity	17 GW_{th}	6 GW_{th} DX systems 8 GW_{th} AC CWS 3 GW_{th} WC CWS
BESS capacity	35 GWh	Net useable capacity
Peak gas generation demand	2.5 GW	Across all scenarios

$$GT^{p} - GT_{p,t} \geq 0, \forall p \in \mathscr{P}, \forall t \in \mathscr{T} \tag{16}$$

2.3.1. I-TES model

While the behavior of individual I-TES tanks is a non-linear function of the state of charge and inlet water-glycol temperature and flowrate, the aggregate behavior of thousands of modular I-TES tanks is approximated by a simple linear function of chiller loading. As seen by the electricity grid, the electric cooling load is altered because of load shifting from using I-TES. The electric load increases when forming ice

Table 6
Cost-optimal system characteristics at \$140/ton of CO_2 carbon price.

Parameter	Value	Notes
Cost	\$2487 million/yr.	Annual cost from Capex and OpEx
Average power generation cost	\$52/MWh	From gas and PV generation
Demand met by gas generation	8%	Mostly In the high-demand season
Demand met by PV generation	40%	Directly
Load shifted by I-TES	23%	All cooling systems
Load met by the BESS	29%	Primarily non-cooling loads
Cooling demand met by PV generation	34%	Directly
Cooling demand met by I-TES	57%	All cooling systems
Cooling demand met by BESS	9%	Mostly In the high-demand season
Solar capacity factor	20%	After curtailment
Curtailment	16%	Of total PV generation
I-TES average capacity utilization	73%	Equivalent full cycle per day
BESS average capacity utilization	92%	Equivalent full cycle per day

and decreases when I-TES is dispatched. The dispatch of I-TES reduces the load on cooling systems proportional to the dispatched amounts and systems COP. The cooling load balance for each system is described by:

$$\mathscr{D}_{p,t}^{DX} = \left(\frac{1}{COP_{p,t}^{ac}}\right)\left[\mathscr{C}_{p,t}^{DX} - S_{p,t,i}^{dis}\right] + \left(\frac{S_{p,t,i}^{ac,chs}}{COP_{p,t}^{ac,ice}}\right), \forall p \in \mathscr{P}, \forall t \in \mathscr{T}, i = 1 \quad (17)$$

$$\mathscr{D}_{p,t}^{AC} = \left(\frac{1}{COP_{p,t}^{ac}}\right)\left[\mathscr{C}_{p,t}^{AC} - S_{p,t,i}^{dis}\right] + \left(\frac{S_{p,t,i}^{ac,chs}}{COP_{p,t}^{ac,ice}}\right), \forall p \in \mathscr{P}, \forall t \in \mathscr{T}, i = 2 \quad (18)$$

$$\mathscr{D}_{p,t}^{WC} = \left(\frac{1}{COP_{p,t}^{wc}}\right)\left[\mathscr{C}_{p,t}^{WC} - S_{p,t,i}^{dis}\right] + \left(\frac{S_{p,t,i}^{ac,chs}}{COP_{p,t}^{ac,ice}}\right) + \left(\frac{S_{p,t,i}^{wc,chs}}{COP_{p,t,i}^{wc,ice}}\right), \forall p \in \mathscr{P}, \forall t \in \mathscr{T}, i = 3 \quad (19)$$

where $\mathscr{C}_{p,t}^{DX}$, $\mathscr{C}_{p,t}^{AC}$, and $\mathscr{C}_{p,t}^{WC}$ is the estimated aggregate thermal cooling demand for the DXS, AC CWS, and WC CWS. The COP of AC and WC systems is $COP_{p,t}^{ac}$ and $COP_{p,t}^{wc}$ in refrigeration mode, and $COP_{p,t}^{ac,ice}$ and $COP_{p,t,i}^{wc,ice}$ in ice-making mode, respectively. $S_{p,t,i}^{ac,chs}$ and $S_{p,t,i}^{wc,chs}$ are I-TES charging rates using AC and WC chillers, respectively, and $S_{p,t,i}^{dis}$ is the ice melt rate of I-TES. The stored thermal energy in the ice is balanced via the following two constraints:

$$S_{p,t,i}^{s} - \eta^{ITES,sdis} S_{p,t-1,i}^{s} = S_{p,t,i}^{ac,chs} + S_{p,t,i}^{wc,chs} - S_{p,t,i}^{dis}, \forall p \in \mathscr{P}, \forall t \in \mathscr{T}, \forall i \in \mathscr{I} \quad (20)$$

$$S_{p,t,i}^{s} \le C_{i}^{ITES}, \forall p \in \mathscr{P}, \forall t \in \mathscr{T}, \forall i \in \mathscr{I} \quad (21)$$

where $S_{p,t,i}^{s}$ is the amount of thermal energy stored in ice and $\eta^{ITES,sdis}$ is the self-discharge efficiency from thermal losses. The amount of dispatchable stored thermal energy is restricted to the available thermal cooling demands:

$$S_{p,t,i}^{dis} \le \mathscr{C}_{p,t}^{DX}, \forall p \in \mathscr{P}, \forall t \in \mathscr{T}, i = 1 \quad (22)$$

$$S_{p,t,i}^{dis} \le \mathscr{C}_{p,t}^{AC}, \forall p \in \mathscr{P}, \forall t \in \mathscr{T}, i = 2 \quad (23)$$

$$S_{p,t,i}^{dis} \le \mathscr{C}_{p,t}^{WC}, \forall p \in \mathscr{P}, \forall t \in \mathscr{T}, i = 3 \quad (24)$$

and due to physical limitations associated with the maximum melt rate:

$$S_{p,t,i}^{dis} \le f^{ITES,dis} C_{i}^{ITES}, \forall p \in \mathscr{P}, \forall t \in \mathscr{T}, \forall i \in \mathscr{I} \quad (25)$$

where $f^{ITES,dis}$ is the maximum discharge rate per unit capacity in h^{-1}. Similarly, I-TES charge rate is bounded by physical limitations associated with the maximum ice build rate as follows:

$$S_{p,t,i}^{wc,chs} + S_{p,t,i}^{ac,chs} \le f^{ITES,chs} C_{i}^{ITES}, \forall p \in \mathscr{P}, \forall t \in \mathscr{T}, \forall i \in \mathscr{I} \quad (26)$$

and to available chillers cooling capacities in the respective cooling system:

$$S_{p,t,i}^{ac,chs} \le C_{i}^{IceChl} \frac{COP_{p,t}^{ac,ice}}{COP_{p,t}^{ac,des}} \psi^{ice}, \forall p \in \mathscr{P}, \forall t \in \mathscr{T}, \forall i \in \{1,3\} \quad (27)$$

$$S_{p,t,i}^{ac,chs} \le \left[C^{AC} - \mathscr{C}_{p,t}^{AC}\right] \frac{COP_{p,t}^{ac,ice}}{COP_{p,t}^{ac}} \psi^{ice} + C_{i}^{IceChl} \frac{COP_{p,t}^{ac,ice}}{COP_{p,t}^{ac,des}} \psi^{ice}, \forall p \in \mathscr{P}, \forall t \in \mathscr{T}, i = 2 \quad (28)$$

$$S_{p,t,i}^{wc,chs} \le \left[C^{WC} - \mathscr{C}_{p,t}^{WC}\right] \frac{COP_{p,t}^{wc,ice}}{COP_{p,t}^{wc}} \psi^{ice}, \forall p \in \mathscr{P}, \forall t \in \mathscr{T}, i = 3 \quad (29)$$

where $f^{ITES,chs}$ is the maximum charge rate per unity capacity in h^{-1}, $COP_{p,t}^{ac,des}$ and $COP_{p,t}^{wc,des}$ are design COP of AC and WC systems, and ψ^{ice} is the depressed chiller capacity factor, which accounts for the loss in chiller cooling capacities from the reduced refrigerant saturation density due to reduced evaporator temperature in ice-making mode. The DXS charge rate is limited by the additionally installed ice chiller capacity. For AC and WC CWS, the charge rate is limited by the combined cooling capacity of idle and additional ice chillers. The first terms in Equations 28 and 29 are the cooling capacity of existing air and water-cooled chiller, where $C^{WC} = C^{WC,des} COP_{p,t}^{wc} / COP_{p,t}^{wc,des}$ and $C^{AC} = C^{AC,des} COP_{p,t}^{ac} / COP_{p,t}^{ac,des}$. The two terms thus determine the idle chillers' capacity that could be used to make ice.

2.3.2. BESS model

Modeling of BESS is less complex than I-TES due to both storing electric energy and the nature of their performance. No consideration is made for the depth of discharge as C^{BESS} is taken to represent the useable capacity. Charge and discharge rates are limited to a 4-h electric battery (power-to-energy capacity ratio of ¼), a standard market product. The following constraints balance the stored energy and restrict charge and discharge rates:

$$\mathscr{B}_{p,t}^{s} - \eta^{BESS,sdis} \mathscr{B}_{p,t-1}^{s} = \eta^{BESS,chs} \mathscr{B}_{p,t}^{chs} - \frac{1}{\eta^{BESS,dis}} \mathscr{B}_{p,t}^{dis}, \forall p \in \mathscr{P}, \forall t \in \mathscr{T} \quad (30)$$

$$\mathscr{B}_{p,t}^{s} \le C^{BESS}, \forall p \in \mathscr{P}, \forall t \in \mathscr{T} \quad (31)$$

$$\mathscr{B}_{p,t}^{dis} + \mathscr{B}_{p,t}^{chs} \le \left(\frac{1}{4}\right) \times C^{BESS}, \forall p \in \mathscr{P}, \forall t \in \mathscr{T} \quad (32)$$

where $\mathscr{B}_{p,t}^{s}$ is the stored electric energy and $\eta^{BESS,sdis}$, $\eta^{BESS,chs}$, and $\eta^{BESS,dis}$ are the self-discharge, charge, and discharge efficiencies, respectively. To prevent simultaneous BESS charging and discharging, a negligibly small cost in the order of 10^{-3} \$/MW is applied to $\mathscr{B}_{p,t}^{chs}$ in the objective function, which does not impact the cost-optimal system.

2.3.3. Model parameters

The considered characteristics parameters in the model are tabulated in Table 1. An efficient inverter with 98% efficiency was assumed for the PV system [68]. A 4-h BESS was considered with charging and discharging efficiencies of 92% and a self-discharge efficiency of 99.9% [69,70]. The charge and discharge efficiencies also account for inverter losses. The modeled I-TES is an internal melt type favored for its modularized construction and predictable charge and discharges behavior. The maximum charge rate of 1/6 h^{-1} and discharge rate of

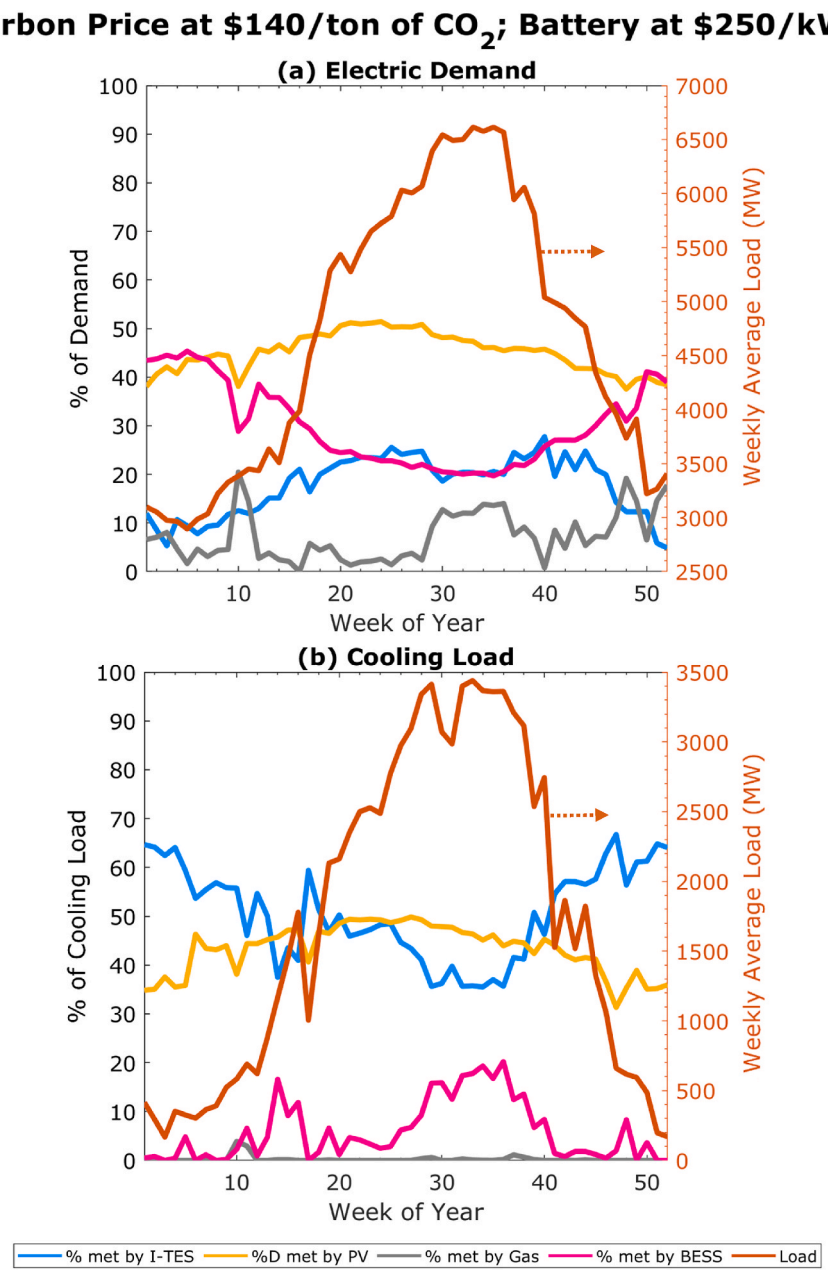

Fig. 16. Cost-optimal system with a carbon price at \$140/ton of CO_2 and BESS capacity cost at \$250/kWh with a breakdown of contribution to supplying (a) the electric demand and (b) the electric cooling load. The electric cooling load is assumed to be met first by PV generation before BESS is used, and the remaining load is met using gas generation.

$1/3\ h^{-1}$ are from performance data from CALMAC, a prominent internal melt I-TES manufacturer. Measurements taken from I-TES demonstrate a high self-discharge efficiency of 99.9% [71].

The reported maximum electric loads from the cooling system by the utility are used to predict the corresponding existing cooling systems' cooling capacities. The design cooling capacities are conservatively assumed to be oversized by 20% above the utility's peak load estimate; this corresponds to AC CWS and WC CWS's maximum electric load of 2.5 and 1.4 GW, respectively. At design WC and AC systems COP of 4.2 and 2.4, respectively, the estimated aggregate thermal cooling capacities are 3.1 GW_{th} for DXS, 6.1 GW_{th} for AC CWS, and 5.7 GW_{th} for WC CWS. The subscript "th" is used to differentiate thermal and electric capacities. ITES and BESS are assumed to be initially fully charged at the first hour of analysis in each scenario (January 1st at midnight) in order not to impede the minimization of peak gas generation demand.

The assumed financial parameters in the model are tabulated in Table 2. All capital costs are installed costs and are taken on the lower side [28,54,62,70,72–75], benefiting from the economy of scale and access to a cheap labor force. OpEx was valued per unit capacity per year and not based on consumption [76–78]. Based on utility-scale prices in Qatar [28], installed PV is at \$450/$kW_{p,dc}$ for fixed-tilt, \$550/$kW_{p,dc}$ for single-axis tracking, and \$700/$kW_{p,dc}$ for dual-axis tracking. OpEx for installed PV was at \$10/$kW_{p,dc}$/yr. for fixed-tilt, \$15/$kW_{p,dc}$/yr. for single-axis tracking, and \$20/$kW_{p,dc}$/yr. for dual-axis tracking. The cost of I-TES was taken to be \$50/TR-hr (\$14/kWh_{th}) [54] and ice chillers at \$200/TR (\$57/kW_{th}) [72,73]. 4-hour BESS was taken at \$250/kWh, of which is \$200/kW for power and \$200/kWh for energy components [70,75]. Gas generation cost of \$37/MWh is averaged over a year and covers all OpEx. Benefiting from access to cheap capital in the region, finances are done at a 3.5% interest rate. Service life of 25 years was assumed for I-TES, ice chillers, and PV and 10 years for the BESS [74,79,80].

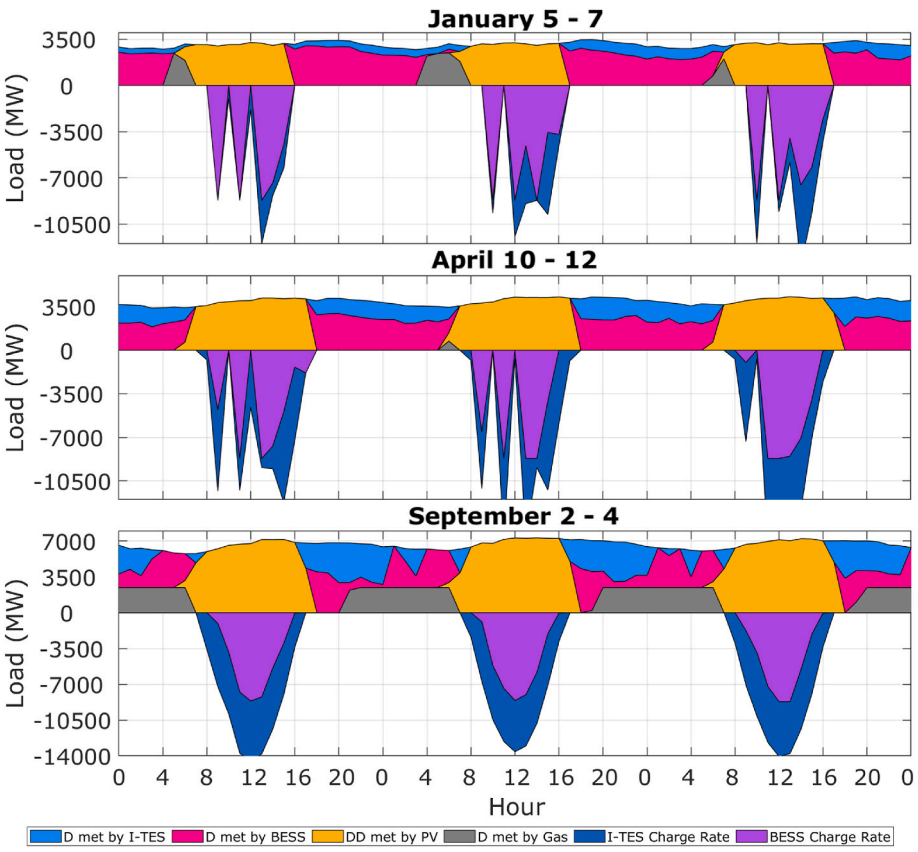

Fig. 17. Cost-optimal system hourly load profile with a carbon price at $140/ton of CO_2 and BESS capacity cost at $250/kWh with contributions from PV generation and load shifting using I-TES and BESS to meet the electric demand for three days in winter, spring, and summer. I-TES and BESS charge rates are shown as negative loads.

3. Results and discussion

First, the formulated problem is solved at the current cost structure to determine the penetration of PV, I-TES, and BESS. Second, the impact of the carbon pricing policy on decarbonization is examined. Third, a deeply decarbonized system supported by carbon pricing is analyzed in detail. Last, the impact of the continual decline in the cost of BESS on the cost-optimal system is investigated. For all considered cases, dual-axis tracking PV was not economically feasible and was omitted from the results.

3.1. Current cost structure

The formulated problem is solved at the current cost structure tabulated in Table 2. The model results suggest that BESS is not cost-effective under current conditions. The cost-optimal system, as tabulated in Table 3, comprises 8.1 $GW_{p,dc}$ of PV capacity (5.9 $GW_{p,dc}$ for fixed-tilt and 2.2 $GW_{p,dc}$ for single-axis tracking), 28 GWh_{th} of aggregate I-TES capacity (3 GWh_{th} for DXS, 15 GWh_{th} for AC CWS, and 10 GWh_{th} for WC CWS), and 0.7 GW_{th} of aggregate ice chillers capacity for the DXS. For AC CWS and WC CWS, I-TES is charged using the existing idle chillers' capacity. Benefiting from optimized load shifting using I-TES during the summer months, peak gas generation demand is reduced by 18% (7.33–6.0 GW).

The cost-optimal system stipulates investing $326 million/yr. in PV capacity, $25 million/yr. in I-TES capacity, and $4 million/yr. in additional ice chillers capacity. This investment brings about a 20% reduction in both the average cost of produced energy ($37/MWh to $29/MWh) and total annual system costs ($1.5 billion/yr. to $1.2 billion/yr.) relative to the current approach of all gas-fired generations by utilizing low-cost energy produced by PV generation.

A PV capacity of 8.1 $GW_{p,dc}$ is slightly higher than the current peak electricity demand of 7.33 GW, producing low-cost electricity to displace gas generation during the day and year-round excess generation for I-TES use. About half of the excess generation is used to store ice, and the remaining half is curtailed. The mismatch between PV generation, which peaks in June, and the cooling load, which peaks in August, is the primary reason for curtailment. The cost-optimal system's preference for fixed-tilt PV generation is due to its lower costs and the lack of energy storage capacity to utilize the higher surplus generation generated with solar tracking technology.

The cost-optimal system characteristics averaged over the four scenarios (2013–2016) are tabulated in Table 4. 38% of the electric demand was directly met by PV generation, and 5% in-directly from load shifting using I-TES. Since power generations in Qatar exclusively use gas generation with collective CO_2 emissions of 24 Mt/yr, the electric demand met by PV and load shifted by I-TES is directly proportional to gas consumption and CO_2 emissions reduction. Gas generation use and CO_2 emissions are reduced by 43%, of which PV alone contributes almost 90% of these emissions reductions.

Fig. 11 shows the weekly average percent contribution of the I-TES, PV, and gas generation in meeting the electric demand in (a) and the electric cooling load in (b). Note that the load met by I-TES corresponds to the electric load shifted. The highest utilization of I-TES is in the low cooling demand season is enabled by a higher amount of surplus PV generation and idle chillers capacity. It reduces the nighttime cooling load by 40–60%, which equates to about load shifting 10% of the nighttime electricity needs. Higher electricity and cooling demand in the warmer season produces less surplus PV generation coupled with a lack of idle chillers capacity constrained and diminished I-TES use. Nonetheless, sole PV generation consistently and reliably met 40% of the cooling load and electric demand. This system decarbonizes 54% of the

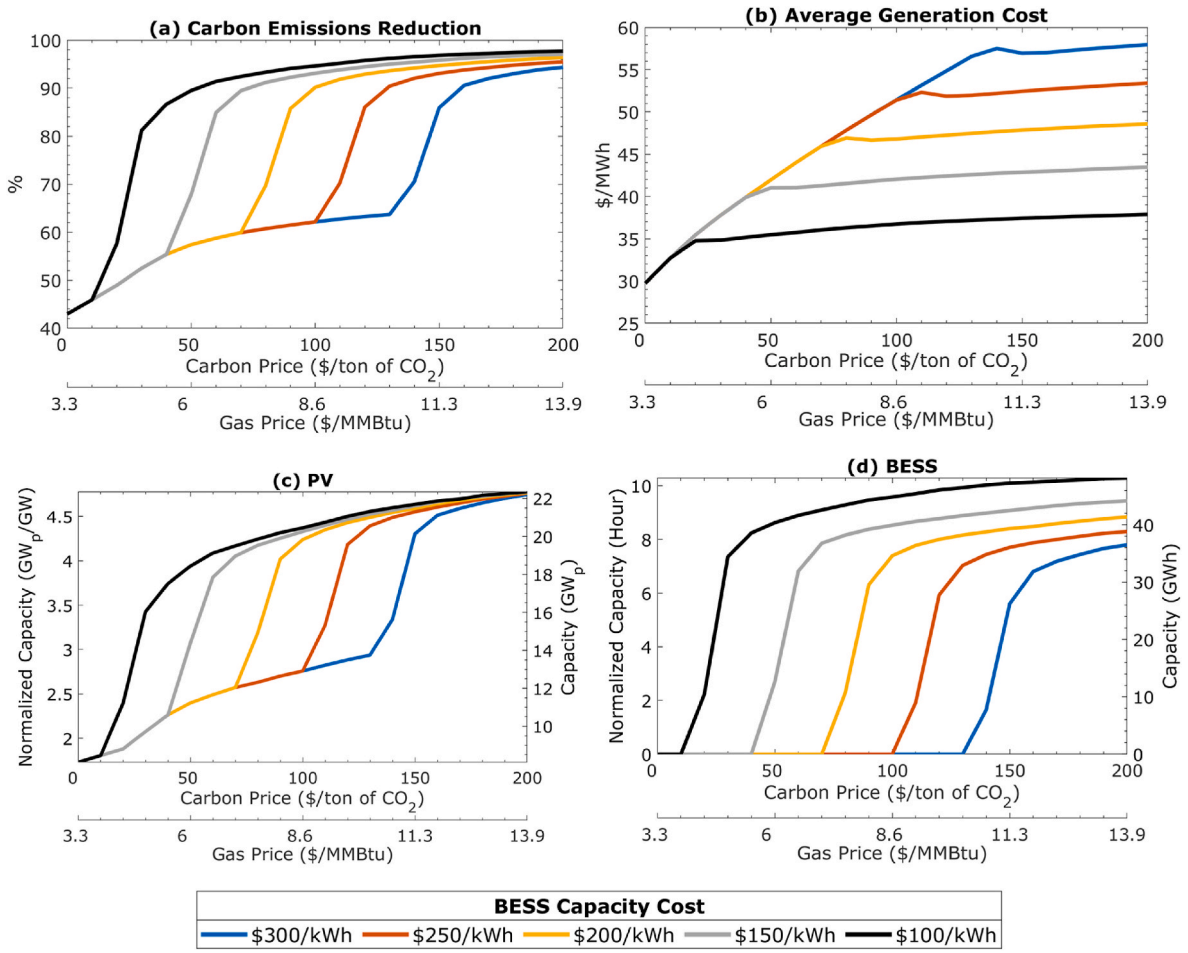

Fig. 18. Impact of BESS capacity cost and carbon pricing on the cost-optimal system with (a) emissions reduction, (b) average generation cost, (c) total PV capacity (fixed-tilt and single-axis tracking), and (d) BESS capacity. PV and BESS capacity is normalized to the 2016 yearly average electric demand of 4.7 GW.

electric cooling load, of which PV directly contributes 41%, and I-TES contributes 13% from cooling load shifting.

The load profile for three consecutive days in the winter, spring, and summer are shown in Fig. 12 for the 2016 scenario, with DD (demand directly) met from PV and D (demand) met by I-TES. In the winter, I-TES is continuously dispatched, restricted by the absence of cooling demand. When the cooling demand has increased in the spring, I-TES is dispatched to displace cooling systems operating at reduced efficiency due to relatively higher dry-bulb temperatures in the AC systems or wet-bulb temperatures in WC CWS. This can be seen from the correlation between the I-TES dispatch amount and higher ambient temperatures. In the summer, I-TES use was limited due to multiple adverse factors: (i) limited idle chillers' capacity for charging due to higher cooling demand, (ii) chillers' cooling capacities degradation from higher ambient temperatures, and (iii) limited amount and duration of surplus PV generation. Still, a smaller amount of stored ice is dispatched in the early evening hours to reduce the peak gas-fired generation demand.

Gas generation, which has to cover intermittent PV generation and lack of storage, sees a high ramp rate of 3.5–5 GW/h (50–70% of the current peak demand) for less than 100 h of the year caused by the early evening peak in the summer. The ramp rates do not exceed 2.5 GW/h for the remaining time. On average, 70% of I-TES capacity is utilized daily, with an average charge residency of 17 h, counterintuitively depressed by lower utilization in the high cooling demand season. Storage is charged in 2500 h, restricted by the narrow charging window, equivalent to the number of hours PV produces surplus power. I-TES is dispatched over 4450 h to reduce gas generation use and peak demand.

3.2. Impacts of carbon pricing

Plentiful and easily accessible natural gas provided low-cost fuel to gas generation in Qatar, instigating a cost structure that lacks the appropriate economic incentives to reduce carbon emissions. This section assesses carbon pricing policy to promote energy and environmental sustainability. The cost-optimal system with a carbon pricing from 0 to $200/ton of CO_2 is shown in Fig. 13 with capacities of power generators in (a), BESS in (b), I-TES in (c), (e), and (g), and ice chillers in (d), (f). and (h) for DXS, AC CWS, and WC CWS, respectively. Fig. 14 (a)-(d) shows the corresponding cost-optimal system characteristics.

The cost-optimal system with carbon pricing below $20/ton of CO_2 is dominated by PV generation and limited I-TES. That is because I-TES cannot outcompete already existing gas generation for highly seasonal cooling needs. This system nearly displaces all daytime gas generation directly using lower-cost PV generation and exploits surplus generation to reduce the nighttime cooling load in the shoulder seasons using I-TES. While fixed-tilt PV generation is initially preferred, fixed-tilt is swapped for single-axis tracking with a net positive gain as the carbon price increases, accompanied by an increase in additional ice chillers and I-TES capacity. PV generation with I-TES for electric and cooling loads decarbonization reaches a plateau at carbon pricing of $100/ton of CO_2. For this system, about 88% of cooling needs are met using PV generation during the daytime and I-TES during the nighttime. The remaining 12% is in days with reduced solar output and during the high cooling load season between July and September. Optimized I-TES dispatch could reduce peak demand from gas generation by 35% (7.33–4.8 GW); further decrease is limited by the non-cooling portion of the electric

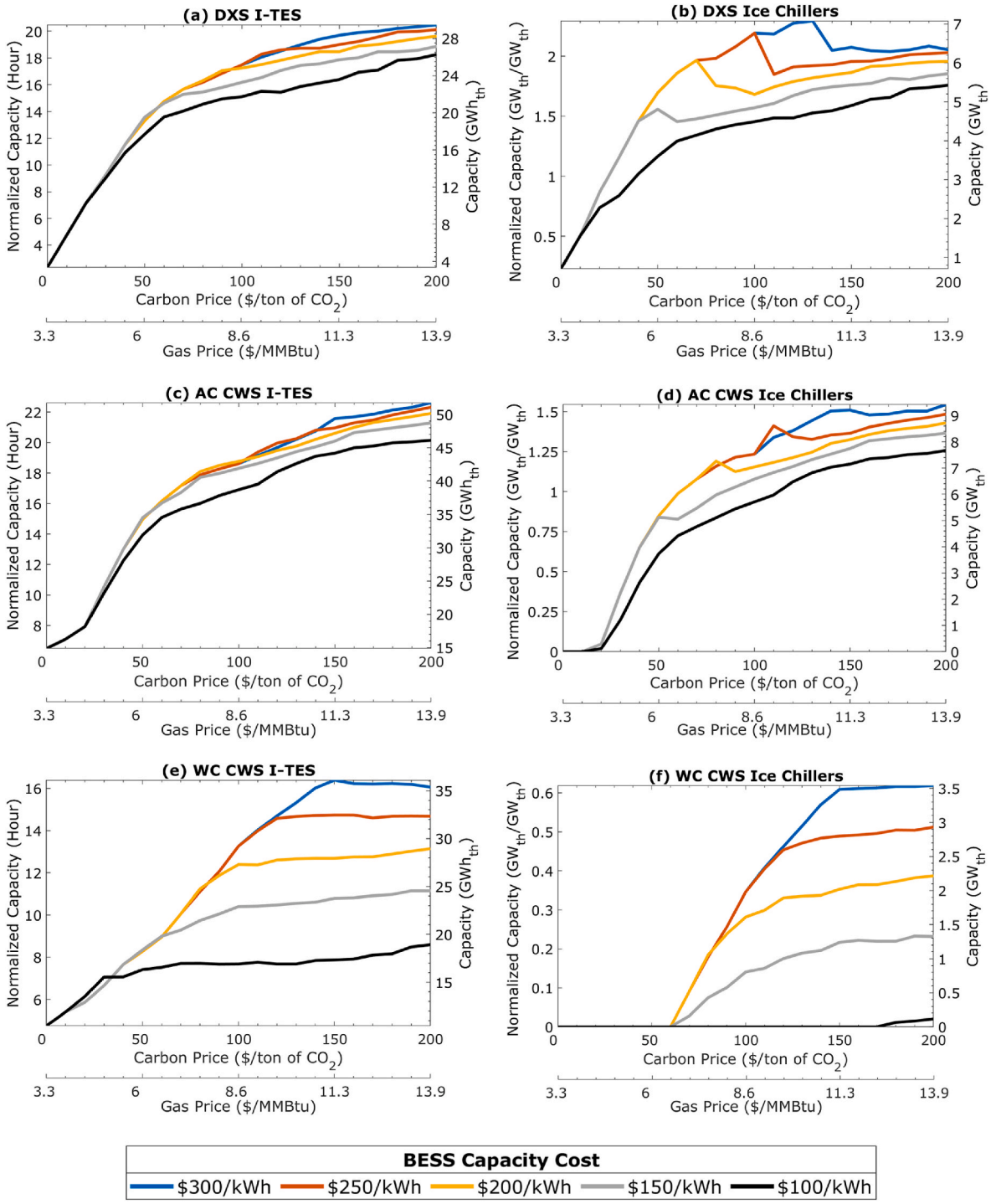

Fig. 19. The impact of BESS capacity cost and carbon pricing on the cost-optimal system. I-TES capacity is normalized to the average aggregate cooling demand of 1.4 GW_{th} for DXS, 2.3 GW_{th} for AC CWS, and 2.2 GW_{th} for WC CWS. Ice chillers' capacity is normalized to the aggregate cooling capacity of 3.1 GW_{th} for DXS, 6.1 GW_{th} for AC CWS, and 5.7 GW_{th} for WC CWS.

demand and challenges of using I-TES in the high cooling load season.

Different cooling system technologies respond differently to carbon pricing. AC systems are favored over WC CWS for I-TES use due to a lower system COP; this means an equal amount of thermal energy corresponds to a greater electric load shifting in AC systems. An additional advantage for AC CWS is utilizing the idle capacity to make ice, allowing for greater penetration of I-TES at reduced costs compared to DXS. To decarbonize nighttime cooling needs, the additional installed ice chillers' capacity is 2, 1.4, and 0.5 times the existing nominal capacities of DXS, AC CWS, and WC CWS, respectively. This large additional capacity is needed because of the capacity loss in ice-making mode and the necessity to store nighttime cooling needs during daylight hours of no more than 6–8 h. Less additional ice chillers are needed in CWS by utilizing the existing idle capacity to make ice. Furthermore, the pronounced difference between AC and WC CWS is due to more minor intra-annual and diurnal variations in ambient wet-bulb than dry-bulb temperatures, corresponding to less capacity degradation and a more consistent cooling system performance.

Several possible approaches can alleviate the challenges of decarbonizing a highly seasonal cooling load, including (i) more considerable reliance on WC systems that are more efficient and experience less cooling capacity degradation; (ii) DXS capable of ice charging in future constructions could allow for higher penetration of I-TES at reduced costs; (iii) more energy-efficient buildings would reduce the seasonality of the cooling and electric loads.

BESS becomes cost-effective above carbon pricing of $100/ton of CO_2. The analysis suggests that BESS does not displace I-TES for cooling load shifting and is primarily used to manage the diurnal behavior of non-cooling loads. BESS requires a high average daily capacity utilization rate of around 90% to be economical, which is unsuitable for a seasonal cooling load. The model suggests a rapid increase in installed BESS capacity with carbon prices up to $140/ton of CO_2. This system achieves a decarbonization rate exceeding 90%, which vastly diminishes the role of gas generation. With a net positive increase in PV generation capacity, the cost-optimal system shifts to a preference for fixed-tilt PV generation over single-axis tracking enabled by BESS's naturally higher charging rate, which reduces system cost and curtailment.

Curtailment remains modest, between 10 and 20% of total PV generation. Unless long-duration energy storage is considered, surplus PV generation produced from the mismatch between electric and cooling loads, which peaks in August, and PV generation, which peaks in June, is curtailed. As carbon pricing increases from 0 to $200/ton of CO_2, the average cost of power generation increases by about a factor of 2 in the cost-optimal systems. At the same time, emissions sharply declined by a factor of 7 relative to the cost-optimal system 12 relatives to the current system structure. Furthermore, the higher annual system costs are increasingly from Capex, driven by installed PV and BESS, as opposed to OpEx from the carbon tax.

The carbon abatement cost, defined as the yearly cost of mitigating carbon emissions from the use of gas generation, for the cost-optimal system as carbon pricing increases is shown in Fig. 15. The negative abatement cost at low carbon pricing indicates that a more sustainable solution can be achieved at a reduced annual cost. Otherwise, the abatement cost does not exceed $55/ton of CO_2 up to a decarbonization rate of nearly 95%, supported by low-cost PV generation combined with the low cost of I-TES and reliable non-cooling load for BESS.

3.3. Decarbonized system with $140/ton of CO_2 carbon tax

This section examines a deeply decarbonized system supported by carbon pricing at $140/ton of CO_2 at the current BESS capacity cost of $250/kWh. Limited carbon emissions reduction can be realized beyond a carbon price of $140/ton of CO_2 using the examined pathway, as shown in Fig. 15. PV generation combined with BESS and I-TES cannot compete with existing gas generation for highly seasonal cooling between mid-July and mid-September. This deeply decarbonized system utilizes PV generation for daytime electric loads, I-TES for nighttime cooling, and BESS for non-cooling electricity needs, achieving a 92% percent reduction in emissions from the current approach of all gas generation.

As tabulated in Table 5, the cost-optimal system comprises 21 $GW_{p,dc}$ of PV (15 $GW_{p,dc}$ for fixed-tilt and 6 $GW_{p,dc}$ for single-axis tracking), 107 GWh_{th} of I-TES (27 GWh_{th} for DXS, 48 GWh_{th} for AC CWS, and 32 GWh_{th} for WC CWS), 17 GW_{th} of additional ice chillers (6 GW_{th} for DXS, 8 GW_{th} for AC CWS, and 3 GW_{th} for WC CWS), and 35 GWh of useable BESS capacity. In AC CWS and WC CWS, I-TES also benefits from utilizing existing idle chillers' capacity for ice-making. However, peak demand from gas generation was only reduced by 66% to 2.5 GW since PV with BESS and I-TES cannot displace gas generation during the peak demand season between mid-July to mid-September.

The cost-optimal system characteristics averaged over the four scenarios are tabulated in Table 6. 40% of the electric demand was directly met by PV generation, and 23% and 29% in-directly from load shifting using I-TES and BESS, respectively. The remaining 8% of the electric demand is met using gas generation with less than 1300 h of operation on days with reduced solar output and peak cooling demand days. Further decarbonization using PV generation might require long-duration energy storage. Due to reliable nighttime cooling and electricity needs, the required PV capacity to decarbonize the system is about three times the current peak electricity demand. Governed by the seasonality of cooling demand, I-TES average daily capacity utilization rate remains around 70%. On the other hand, The capacity factor for BESS is higher at 92%, suggesting continual year-round use for managing the non-cooling load.

The cost-optimal system increases the average cost of produced energy by 41% ($37/MWh to $52/MWh) and total annual system cost by 65% ($1.5 billion/yr. to $2.5 billion/yr.) relative to the current approach of all gas-fired generation. The cost-optimal system incurs $845 million/yr. from installed PV, $92 million/yr. from installed I-TES, $107 million/yr. from additional ice chillers, and $1047 million/yr. from installed BESS capacity. Annual gas generation expenditure was reduced to $383 million/yr. The percent contribution of PV, I-TES, BESS, and gas generation to meet the electric demand and electric cooling load is shown in Fig. 16. I-TES became a prominent year-round contributor to meeting the electric demand, especially during the high cooling season. BESS, on the other hand, contributes to meeting cooling loads in the high-demand season. However, BESS contributes a steady amount of energy to the electricity grid year-round to meet the baseload.

Hourly system loads for three consecutive days in the winter, spring, and summer are shown in Fig. 17. BESS is dispatched overnight to manage the non-cooling load. In the peak season, I-TES and BESS are dispatched to minimize gas generation use and peak demand. The sole use of PV generation for energy storage charging in the deeply decarbonized system soars the daytime electric load to 15–20 GW compared to the current daytime load of 5–7 GW.

3.4. Impact of BESS capacity cost

BESS remains cost-prohibitive at the capacity cost of $250/kWh without economic incentives. However, the continual decline in the capacity cost can enable BESS to be cost-effective at a reduced carbon price to decarbonize non-cooling loads. This section investigates the impact of the BESS capacity cost and carbon pricing on the cost-optimal system. For comparison, the assumed ice chiller, I-TES, and PV CapEx only minorly influence the cost-optimal system, partly due to their ability to compete with gas generation at the current cost structure. The cost-optimal system for a BESS capacity cost ranging from $100/kWh to $300/kWh and carbon pricing between 0 and $200/ton of CO_2 is shown in Fig. 18 with (a) emissions reduction, (b) generation cost, (c) total PV capacity, and (d) BESS capacity. Cooling systems characteristics are shown in Fig. 19 with I-TES and chillers capacities for DXS, AC CWS, and WC CWS, respectively.

Similar to the outcome from the analysis with carbon pricing, the model suggests that a declining BESS capacity cost will not displace the use of I-TES for cooling load shifting even as the capacity cost is considerably dropped to $100/kWh but will increasingly utilize BESS to supplement seasonal cooling needs. This is seen as a drop in I-TES and chillers capacities in Fig. 19 and is necessary to maintain a cost-effective BESS with a bigger capacity. In CWS, more idle chiller capacities are utilized for I-TES charging in the shoulder season, supported by the higher availability of surplus PV generation without additional ice chiller capacities. As BESS cost declines, WC CWS sees a more significant drop in I-TES and chillers capacity than AC CWS and DXS. As indicated earlier, stored thermal energy corresponds to less electric load shifting in WC systems due to a higher system COP, making BESS more cost-competitive.

Reducing BESS capacity costs promotes using more BESS with a limited need for an additional PV capacity. The BESS partly substitutes I-TES in the high-demand season with a higher round trip efficiency of about 85% compared to 60–70% in I-TES. Furthermore, as the capacity

cost is reduced to $100/kWh, the average cost of produced energy in a deeply decarbonized system could approach that of the current cost of gas generation of $37/MWh. However, the annual cost remains moderately higher at $1.8 billion/yr. due to round-trip losses compared to the current system cost of $1.5 billion/yr.

4. Conclusion

High electricity demand from space-cooling that is predictable and synergetic with high solar insolation provides a unique opportunity to exploit solar PV-enabled decarbonization solutions in Qatar. The study examined the economic viability of using utility-scale solar PV generation combined with centralized BESS for electric load shifting and decentralized building-scale I-TES for cooling load shifting. The problem was formulated in a two-stage stochastic linear programming that minimizes annual system costs at a given gas price. Statistical tools were used to estimate electric demand due to space cooling from correlations with ambient conditions.

With the aid of carbon pricing through governmental action, the study establishes cost-effective measures to decarbonize the electricity sector in Qatar. The outcomes of the study are summarized in the following six points:

i. Under the current cost structure, CO_2 emissions and peak gas generation demand could be reduced by 43% and 18%, respectively, while cutting annual system costs by 20%.
ii. Without carbon pricing, I-TES is counterintuitively primarily used in low cooling demand seasons by utilizing idle chillers, whereas in the summer, I-TES use is constrained by the availability of surplus PV generation and chiller capacity for ice-making.
iii. Challenges are confronted when applying carbon pricing to decarbonize the electricity sector due to multiple adverse factors, including (i) both cooling and non-cooling demands peak in August, whereas PV generation peaks in June, producing less surplus generation in the time of need; (ii) I-TES for highly seasonal cooling needs cannot cost-effectively outcompete already existing gas generations; (iii) reduced idle chiller capacity during peak cooling demand season due to higher ambient temperatures and cooling demand.
iv. The cost-optimal system at a gas price of less than $8.6/MMBtu (carbon pricing at $100/ton of CO_2) is dominated by PV and I-TES and could reduce emissions by 40–60%, of which I-TES contributes between 5 and 15%.
v. BESS becomes cost-effective above a gas price of $9.2/MMBtu (carbon pricing above $100/ton of CO_2) and is primarily used to manage the reliable non-cooling demand.
vi. A system with a gas price of $10.8/MMBtu (carbon pricing at $140/ton of CO_2) could fully decarbonize the cooling load and reduce CO_2 emissions by 92%.

However, several approximations and estimations were made throughout this work that are likely to limit the outcomes of this study, including:

i. The estimated cooling loads served by each cooling system technology are unlikely to be perfectly correlated, as assumed, which might affect the amount of storage needed.
ii. The COP of cooling systems is a more complex function of ambient and evaporator temperature, loading, and construction than estimated.
iii. The simplified linear I-TES model does not perfectly represent the complex physics of ice formation and melting inside the I-TES.

In short, by using existing decarbonization solutions at current installed prices, the power utility in Qatar could substantially reduce its carbon footprint and decrease the reliance on gas generation using centralized PV generation and BESS, building-scale I-TES, and implementing carbon pricing. Future research questions are raised about the complexity and challenges of the site installation and operation of I-TES and the challenges of maintaining a reliable power grid with a high penetration of non-dispatchable generation.

Credit author statement

Ibraheam Al-Aali (PhD candidate), Second author: Dr. Vijay Modi (advisor).

Declaration of competing interest

The authors declare the following financial interests/personal relationships which may be considered as potential competing interests: Ibraheam Ali Al-Aali reports financial support was provided by Qatar National Research Fund.

Data availability

The authors do not have permission to share data.

Acknowledgments

This research was sponsored by Qgrants thru Qatar National Research Fund (QNRF) with grant number QRLP10-G-1803028. The authors of this paper would also like to show gratitude to Qatar General Electricity and Water Corporation (Kahramaa) for providing the necessary power generation data and to Qatar Environment and Energy Institute (QEERI) for providing the hourly solar irradiance data that allowed this work to be possible.

References

[1] Qatar - Countries & Regions - IEA, 2019 [Online]. Available: https://www.iea.org/countries/qatar. (Accessed 25 July 2022). Accessed.
[2] Kahramaa, Annual Qatar Statistics Report, 2016, 2016.
[3] F. Saffouri, I.S. Bayram, M. Koc, Quantifying the Cost of Cooling in Qatar, February, 2018, pp. 1–9, https://doi.org/10.1109/ieeegcc.2017.8448269.
[4] I.S. Bayram, F. Saffouri, M. Koc, Generation, analysis, and applications of high resolution electricity load profiles in Qatar, J. Clean. Prod. 183 (2018) 527–543, https://doi.org/10.1016/j.jclepro.2018.02.084.
[5] Kahramaa, "Tariff,", Kahramaa [Online]. Available: https://www.km.com.qa/CustomerService/Pages/Tariff.aspx, 2019. (Accessed 3 October 2019). Accessed.
[6] S.G. Al-Ghamdi, S.K. Al-Thani, QCCC (2021).
[7] E.S. Fadala, Raffaello, Sustainable neighborhoods in the state of Qatar: msheireb downtown doha, Saudi J. Eng. Technol. 3 (7) (2018) 446–463, https://doi.org/10.21276/sjeat.2018.3.7.2.
[8] New Qatari Standards for AC Energy Efficiency, Kahramaa, in: Efficiency System Contains,12%25 Compared with Unclassified Appliance, 2013 [Online]. Available: https://www.km.qa/MediaCenter/Pages/NewsDetails.aspx?itemid=18#:~:text=Qatarienergy. (Accessed 25 July 2022) [Accessed.
[9] A. Meier, M. Darwish, S. Sabeeh, Complexities of Saving Energy in Qatar," *ECEEE 2013 Summer Study Proc*, 2013, pp. 41–46.
[10] Amjad Khashman, Qatari Utility Mulls Jump to 800 MW Tender as Consortia Submit Bids, PV Magazine, 2019.
[11] Tassal Group Limited, Sustainability Report 2020, Doha, 2020.
[12] M.A. Bohra, Optimising Qatar's Energy Transition through Model-Based Analysis," No, March, 2020.
[13] M. Bohra, N. Shah, Optimising the role of solar PV in Qatar's power sector, Energy Rep. 6 (2020) 194–198, https://doi.org/10.1016/j.egyr.2019.11.062.
[14] L. Martín-Pomares, D. Martínez, J. Polo, D. Perez-Astudillo, D. Bachour, A. Sanfilippo, Analysis of the long-term solar potential for electricity generation in Qatar, Renew. Sustain. Energy Rev. 73 (2017) 1231–1246, https://doi.org/10.1016/j.rser.2017.01.125. March 2016.
[15] E.C. Okonkwo, I. Wole-Osho, O. Bamisile, M. Abid, T. Al-Ansari, Grid integration of renewable energy in Qatar: potentials and limitations, Energy 235 (2021), 121310, https://doi.org/10.1016/j.energy.2021.121310.
[16] A.H. Marafia, H.A. Ashour, Economics of off-shore/on-shore wind energy systems in Qatar, Renew. Energy 28 (12) (2003) 1953–1963, https://doi.org/10.1016/S0960-1481(03)00060-0.
[17] O. Alrawi, I.S. Bayram, M. Koc, S.G. Al-Ghamdi, Economic viability of rooftop photovoltaic systems and energy storage systems in Qatar, Energies 15 (9) (2022), https://doi.org/10.3390/en15093040.

[18] N. Elbeheiry, A. Amer, S. Elgazar, S. Shukri, M. Metry, R.S. Balog, A techno-economic study of rooftop grid-connected photovoltaic-energy storage systems in Qatar, Conf. Rec. IEEE Photovolt. Spec. Conf. (2020) 2730–2736, https://doi.org/10.1109/PVSC45281.2020.9300347, 2020-June.
[19] O.F. Alrawi, T. Al-Siddiqi, A. Al-Muhannadi, A. Al-Siddiqi, S.G. Al-Ghamdi, Determining the influencing factors in the residential rooftop solar photovoltaic systems adoption: evidence from a survey in Qatar, Energy Rep. 8 (2022) 257–262, https://doi.org/10.1016/j.egyr.2022.01.064.
[20] E.A. Teshnizi, M. Jahangiri, A.A. Shamsabadi, L.M. Pomares, A. Mostafaeipour, M. El Haj Assad, Comprehensive energy-econo-enviro (3E) analysis of grid-connected household scale wind turbines in Qatar, Jordan J. Mech. Ind. Eng. 15 (2) (2021) 215–231.
[21] İ.Ş. Bayram, M. Koç, Demand side management for peak reduction and PV integration in Qatar, Proc. 2017 IEEE 14th Int. Conf. Networking, Sens. Control. ICNSC (2017) 251–256, https://doi.org/10.1109/ICNSC.2017.8000100, 2017.
[22] M. Krarti, F. Ali, A. Alaidroos, M. Houchati, Macro-economic benefit analysis of large scale building energy efficiency programs in Qatar, Int. J. Sustain. Built Environ. 6 (2) (2017) 597–609, https://doi.org/10.1016/j.ijsbe.2017.12.006.
[23] N. Ayoub, F. Musharavati, S. Pokharel, H.A. Gabbar, Energy consumption and conservation practices in Qatar - a case study of a hotel building, Energy Build. 84 (2014) 55–69, https://doi.org/10.1016/j.enbuild.2014.07.050.
[24] A. Kamal, S.G. Al-Ghamdi, M. Koç, Role of energy efficiency policies on energy consumption and CO2 emissions for building stock in Qatar, J. Clean. Prod. 235 (2019) 1409–1424, https://doi.org/10.1016/j.jclepro.2019.06.296.
[25] A. Abdallah, D. Martinez, B. Figgis, O. El Daif, Performance of silicon heterojunction photovoltaic modules in Qatar climatic conditions, Renew. Energy 97 (2016) 860–865, https://doi.org/10.1016/j.renene.2016.06.044.
[26] D. Martinez-Plaza, A. Abdallah, B.W. Figgis, T. Mirza, Performance improvement techniques for photovoltaic systems in Qatar: results of first year of outdoor exposure, Energy Proc. 77 (2015) 386–396, https://doi.org/10.1016/j.egypro.2015.07.054.
[27] F. Tahir, A.A.B. Baloch, S.G. Al-Ghamdi, Impact of climate change on solar monofacial and bifacial Photovoltaics (PV) potential in Qatar, Energy Rep. 8 (2022) 518–522, https://doi.org/10.1016/j.egyr.2022.02.197.
[28] Kahramaa, The large-scale solar PV power plant [Online]. Available: https://www.km.qa/MediaCenter/Publications/solarEngscreen-min.pdf, 2022.
[29] C. Carpenter, QatarEnergy Picks Samsung C&T to Build Solar Plants to Power its LNG Expansion, S&P Global, 2022 [Online]. Available: https://www.spglobal.com/commodityinsights/en/market-insights/latest-news/electric-power/082322-qatarenergy-picks-samsung-c-t-to-build-solar-plants-to-power-its-lng-expansion. (Accessed 22 August 2022). Accessed.
[30] E. Campiglio, Beyond carbon pricing: the role of banking and monetary policy in financing the transition to a low-carbon economy, Ecol. Econ. 121 (2016) 220–230, https://doi.org/10.1016/j.ecolecon.2015.03.020.
[31] E. Tvinnereim, M. Mehling, Carbon pricing and deep decarbonisation, Energy Pol. 121 (2018) 185–189, https://doi.org/10.1016/j.enpol.2018.06.020. November 2017.
[32] J. Hirwa, O. Ogunmodede, A. Zolan, A.M. Newman, Optimizing design and dispatch of a renewable energy system with combined heat and power, Optim. Eng. (2022), https://doi.org/10.1007/s11081-021-09674-4.
[33] M. Rabe, Y. Bilan, K. Widera, L. Vasa, Application of the linear programming method in the construction of a mathematical model of optimization distributed energy, Energies 15 (5) (2022), https://doi.org/10.3390/en15051872.
[34] I. El Kafazi, R. Bannari, E.B.E.I. Adiba, H. Nabil, T. Dragicevic, Renewable energies: modeling and optimization of production cost, Energy Proc. 136 (2017) 380–387, https://doi.org/10.1016/j.egypro.2017.10.267.
[35] X. Luo, C.K. Lee, W.M. Ng, S. Yan, B. Chaudhuri, S.Y.R. Hui, Use of adaptive thermal storage system as smart load for voltage control and demand response, IEEE Trans. Smart Grid 8 (3) (2017) 1231–1241, https://doi.org/10.1109/TSG.2015.2513743.
[36] S. Al-Hallaj, S. Khateeb, A. Aljehani, M. Pintar, Thermal energy storage for smart grid applications, AIP Conf. Proc. (1924) 2018, https://doi.org/10.1063/1.5020287.
[37] M. MacCracken, Energy storage: providing for a low-carbon future, ASHRAE J. 52 (9) (2010) 28–36.
[38] I. Al-Aali, V. Modi, Examining ice storage and solar PV as a potential push toward sustainability for Qatar, in: ASME International Mechanical Engineering Congress and Exposition, Proceedings (IMECE), 2018, pp. 6B–2018B, https://doi.org/10.1115/IMECE2018-86709.
[39] Y. Ruan, Q. Liu, Z. Li, J. Wu, Optimization and analysis of Building Combined Cooling, Heating and Power (BCHP) plants with chilled ice thermal storage system, Appl. Energy 179 (2016) 738–754, https://doi.org/10.1016/j.apenergy.2016.07.009.
[40] Y. Xu, et al., Experimental investigation of solar photovoltaic operated ice thermal storage air-conditioning system, Int. J. Refrig. 86 (2018) 258–272, https://doi.org/10.1016/j.ijrefrig.2017.11.035.
[41] Y. Han, B. Shen, H. Hu, F. Fan, Optimizing the performance of ice-storage systems in electricity load management through a credit mechanism: an analytical work for Jiangsu, China, Energy Proc. 61 (2014) 2876–2879, https://doi.org/10.1016/j.egypro.2014.12.327.
[42] S.E. Lenker, Building for the future, Stand. News 40 (2) (2012) 34–37, https://doi.org/10.1080/0005576x.1949.11750770.
[43] T. Deetjen, A. Reimers, M.E. Webber, Can storage reduce electricity consumption? A general equation for the grid-wide efficiency impacts of using cooling thermal energy storage for load shifting, Environ. Res. Lett. (2018), https://doi.org/10.1016/j.pepi.2007.08.007.
[44] D. Gräf, et al., What drives capacity degradation in utility-scale battery energy storage systems? The impact of operating strategy and temperature in different grid applications, J. Energy Storage 47 (March 2021) 2021, https://doi.org/10.1016/j.est.2021.103533.
[45] A.M. Ershad, F. Ueckerdt, R.C. Pietzcker, A. Giannousakis, G. Luderer, A further decline in battery storage costs can pave the way for a solar PV-dominated Indian power system, Renew. Sustain. Energy Transit. 1 (May) (2021), 100006, https://doi.org/10.1016/j.rset.2021.100006.
[46] E. Virguez, X. Wang, D. Patiño-Echeverri, Utility-scale photovoltaics and storage: decarbonizing and reducing greenhouse gases abatement costs, Appl. Energy 282 (October 2020) 2021, https://doi.org/10.1016/j.apenergy.2020.116120.
[47] A.H. Schleifer, C.A. Murphy, W.J. Cole, P.L. Denholm, The evolving energy and capacity values of utility-scale PV-plus-battery hybrid system architectures, Adv. Appl. Energy 2 (2021), 100015, https://doi.org/10.1016/j.adapen.2021.100015. March.
[48] M. Arbabzadeh, R. Sioshansi, J.X. Johnson, G.A. Keoleian, The role of energy storage in deep decarbonization of electricity production, Nat. Commun. 10 (1) (2019), https://doi.org/10.1038/s41467-019-11161-5.
[49] N.A. Sepulveda, J.D. Jenkins, F.J. de Sisternes, R.K. Lester, The role of firm low-carbon electricity resources in deep decarbonization of power generation, Joule 2 (11) (2018) 2403–2420, https://doi.org/10.1016/j.joule.2018.08.006.
[50] G. Baure, M. Dubarry, Battery durability and reliability under electric utility grid operations: 20-year forecast under different grid applications, J. Energy Storage 29 (April) (2020), 101391, https://doi.org/10.1016/j.est.2020.101391.
[51] Y. Wu, Z. Liu, J. Liu, H. Xiao, R. Liu, L. Zhang, Optimal battery capacity of grid-connected PV-battery systems considering battery degradation, Renew. Energy 181 (2022) 10–23, https://doi.org/10.1016/j.renene.2021.09.036.
[52] X. Han, J. Garrison, G. Hug, Techno-economic analysis of PV-battery systems in Switzerland, Renew. Sustain. Energy Rev. 158 (2022), 112028, https://doi.org/10.1016/j.rser.2021.112028.
[53] M.S. Ziegler, J.E. Trancik, Re-examining rates of lithium-ion battery technology improvement and cost decline, Energy Environ. Sci. 14 (4) (2021) 1635–1651, https://doi.org/10.1039/d0ee02681f.
[54] Pacific Gas, Electric Company, Thermal Energy Storage Strategies for Commercial HVAC Systems, 1997.
[55] T.B. Jekel, Modeling of Ice-Storage Systems, 1991.
[56] K.H. Drees, Modeling and Control of Area Constrained Ice Storage Systems, Purdue University, West Lafayette, 1994.
[58] T.A. Deetjen, J.S. Vitter, A.S. Reimers, M.E. Webber, Optimal dispatch and equipment sizing of a residential central utility plant for improving rooftop solar integration, Energy 147 (2018) 1044–1059, https://doi.org/10.1016/j.energy.2018.01.110.
[59] I. Al-Aali, A. Narayanaswamy, V. Modi, A novel algorithm for optimal equipment scheduling and dispatch of chilled water systems with ice thermal storage, Energy Build. 274 (2022), 112422, https://doi.org/10.1016/j.enbuild.2022.112422.
[60] S. Hanson, M. Schwedler, B. Bakkum, Chiller System Design and Control, 2011.
[61] Evapco, Thermal Ice Storage, 2007, pp. 3–66.
[62] Federal Energy Management Program, Thermal Energy Storage for Space Cooling Technology for Reducing On-Peak Electricity Demand and Cost, 2000.
[63] Y. Hida, S. Shibutani, M. Amano, N. Maehara, District cooling plant with high efficiency chiller and ice storage system, Mitsubishi Heavy Ind. Ltd. Tech. Rev. 45 (2) (2008) 37–44.
[64] B. Silvetti, Application fundamentals of ice-based thermal storage, ASHRAE J. 44 (2) (2002) 30–35.
[65] P. Denholm, S. Ong, C. Booten, Using Utility Load Data to Estimate Demand for Space Cooling and Potential for Shiftable Loads, 2012.
[66] I.M. Al-Sada, Towards Cooperative District Cooling Society Role of District Cooling Services Department- Opportunities of DC in Qatar, 2014.
[67] M.Z. Jacobson, V. Jadhav, World estimates of PV optimal tilt angles and ratios of sunlight incident upon tilted and tracked PV panels relative to horizontal panels, Sol. Energy 169 (April) (2018) 55–66, https://doi.org/10.1016/j.solener.2018.04.030.
[68] R. Dogga, M.K. Pathak, Recent trends in solar PV inverter topologies, Sol. Energy 183 (2019) 57–73, https://doi.org/10.1016/j.solener.2019.02.065. March.
[69] A.C. Hua, B.Z. Syue, Charge and Discharge Characteristics of Lead-Acid Battery and LiFePO4 Battery, 2010, pp. 1478–1483.
[70] K. Mongird, V. Viswanathan, J. Alam, C. Vartanian, V. Sprenkle, P. Northwest, Grid Energy Storage Technology Cost and Performance Assessment, 2020. December, 2020.

[71] D.S. Christian Weber, Stroupe Ryan, Performance of a thermal energy storage system, 25 Years on, in: Performance of a Thermal Energy Storage System vol. 25, 2015, p. 27.
[72] FPL, Water-Cooled Chiller Characteristics, 2012, pp. 1–4.
[73] Mark Stehney, Air- versus Water-Cooled Chilled Water Plants, 2020 [Online]. Available: https://www.csemag.com/articles/air-versus-water-cooled-chilled-water-plants/. (Accessed 8 November 2022). Accessed.
[74] S. Sabihuddin, A.E. Kiprakis, M. Mueller, A numerical and graphical review of energy storage technologies, Energies 8 (1) (2015) 172–216, https://doi.org/10.3390/en8010172.
[75] W. Cole, A.W. Frazier, C. Augustine, W. Cole, A.W. Frazier, C. Augustine, Cost Projections for Utility-Scale Battery Storage : 2021 Update Cost Projections for Utility-Scale Battery Storage : 2021 Update," No, June, 2021.
[76] D. Feldman, et al., U.S. Solar photovoltaic system and energy storage cost benchmark: q1 2020, *Natl. Renew. Energy Lab.*, no. September (2021) 1–120.
[77] J.H.K. Lai, F.W.H. Yik, A.K.P. Chan, Maintenance cost of chiller plants in Hong Kong, Build. Serv. Eng. Technol. 30 (1) (2009) 65–78, https://doi.org/10.1177/0143624408096290.
[78] Compare - O&M. Costs - Chillers, *Apogee Interactive Inc*. [Online]. Available: https://c03.apogee.net/mvc/home/hes/land/el?spc=cel&id=19018&utilityname=northwestern. (Accessed 4 October 2019). Accessed.
[79] R. Carnegie, D. Gotham, D. Nderitu, P.V. Preckel, Utility Scale Energy Storage Systems, 2013.
[80] J. Ahlen, T. Binet, P. Muhoro, Brad Seibert, Battery Energy Storage Overview, 2019.